The dependence of shugoshin on Bub1-kinase activity is dispensable for the maintenance of spindle assembly checkpoint response in *Cryptococcus neoformans*

Satya Dev Polisetty[1], Krishna Bhat[1], Kuladeep Das[1], Ivan Clark[2], Kevin Hardwick[2], Kaustuv Sanyal[1, 3*]

[1]Molecular Mycology Laboratory, Molecular Biology and Genetics Unit, Jawaharlal Nehru Centre for Advanced Scientific Research, Bengaluru, India.
[2]Institute of Cell Biology, University of Edinburgh, Edinburgh, United Kingdom.
[3]Department of Biological Sciences, Bose Institute, EN 80, Sector V, Bidhannagar, Kolkata, India

*Corresponding author

Kaustuv Sanyal

[1]Molecular Mycology Laboratory, Molecular Biology and Genetics Unit, Jawaharlal Nehru Centre for Advanced Scientific Research, Bengaluru 560064, India. Email: sanyal@jncasr.ac.in
[3]Department of Biological Sciences, Bose Institute, EN 80, Sector V, Bidhannagar, Kolkata 700091, India. Email: sanyal@jcbose.ac.in

Key Words

Chromosome segregation, kinetochore-microtubule attachments, spindle assembly checkpoint (SAC), checkpoint maintenance, *Cryptococcus neoformans*, spindle pole body (SPB).

Abstract

During chromosome segregation, the spindle assembly checkpoint (SAC) detects errors in kinetochore-microtubule attachments. Timely activation and maintenance of the SAC until defects are corrected is essential for genome stability. Here, we show that shugoshin (Sgo1), a conserved tension-sensing protein, ensures the maintenance of SAC signals in response to unattached kinetochores during mitosis in a basidiomycete budding yeast *Cryptococcus neoformans*. Sgo1 maintains optimum levels of Aurora B kinase ^{Ipl1} and protein phosphatase 1 (PP1) at kinetochores. The absence of Sgo1 results in the loss of Aurora B^{Ipl1} with a concomitant increase in PP1 levels at kinetochores. This leads to a premature reduction in the kinetochore-bound Bub1 levels and early termination of the SAC signals. Intriguingly, the kinase function of Bub1 is dispensable for shugoshin's subcellular localization. Sgo1 is predominantly localized to spindle pole bodies (SPBs) and along the mitotic spindle with a minor pool at kinetochores. In the absence of proper kinetochore-microtubule attachments, Sgo1 reinforces the Aurora B kinase^{Ipl1}-PP1 phosphatase balance, which is critical for prolonged maintenance of the SAC response.

Introduction

The precise segregation of duplicated chromosomes in mitosis depends on the stable attachment of kinetochores with microtubules (MTs) and proper orientation on the mitotic spindle. The kinetochore is a multi-subunit protein complex composed of inner and outer layers (Musacchio and Desai, 2017). The inner kinetochore assembles onto centromeric chromatin and is constitutively associated with DNA. Subsequently, the outer kinetochore assembles and promotes the attachment of MTs emanating from microtubule organizing centers: centrosomes in animals or spindle pole bodies (SPBs) in yeast species. Apart from playing a role in MT attachment, the kinetochore also acts as a signaling platform for recruiting mitotic surveillance components that detect unattached or improperly attached kinetochores (Lara-Gonzalez et al., 2021, Zich and Hardwick, 2010, Musacchio and Salmon, 2007). Once errors are detected, cells remain arrested at metaphase until rectified.

Mitotic surveillance systems monitoring erroneous kinetochore-MT attachments include the spindle assembly checkpoint (SAC) and a chromosome passenger complex (CPC) component, Aurora B^{Ipl1}. The SAC comprises Mad1, Mad2, BubR1, Bub3, and the kinases Bub1 and Mps1 (Lara-Gonzalez et al., 2021). The SAC machinery conveys a 'wait anaphase' signal (MCC, the mitotic checkpoint complex) during cell division in response to unattached kinetochores that inhibits the anaphase-promoting complex (APC/C^{Cdc20}) from ubiquitylating B-type cyclins and securin (Hardwick et al., 2000, Musacchio, 2015, Sudakin et al., 2001). Upon the formation of proper kinetochore-MT attachments, the SAC is silenced. APC/C^{Cdc20} inhibition is relieved, resulting in the degradation of B-type cyclins and securin, thus promoting mitotic exit and sister chromatid separation (Cohen-Fix et al., 1996, King et al., 1996).

Tension across sister-kinetochores attached to MTs is important in ensuring high fidelity of chromosome segregation. Tensionless kinetochore-MT attachments, if not rectified, result in the missegregation of chromosomes. Aurora B^{Ipl1} acts as a tension sensor, detecting tension across sister kinetochores (Biggins and Murray, 2001, Tanaka et al., 2002, Hauf et al., 2003, Pinsky et al., 2006). In response to tensionless kinetochore-MT attachments, phosphorylation of outer kinetochore by Aurora B^{Ipl1} results in the destabilization of kinetochore-MT interactions, leading to the generation of unattached kinetochores (Cheeseman et al., 2006, Ciferri et al., 2008) indirectly

activating the SAC. Several reports implicate that Aurora B^{Ipl1} can also directly activate the SAC machinery in response to unattached kinetochores, indicating that the function of Aurora B^{Ipl1} is not just limited to detecting tensionless attachments (Kallio et al., 2002, Petersen and Hagan, 2003, Saurin et al., 2011, Santaguida et al., 2011, Pinsky et al., 2009). The kinase activity of Aurora B^{Ipl1} also counteracts PP1 phosphatase recruitment to kinetochores (Liu et al., 2010). The activity of PP1 at kinetochores is required to terminate the SAC signaling and to help cells proceed into anaphase. PP1 dephosphorylates kinetochore substrates and thus promotes the stabilization of kinetochore-MT attachments (Lara-Gonzalez et al., 2021). Premature recruitment of PP1 to kinetochores results in early termination of SAC signals and leads to chromosome missegregation (Roy et al., 2019).

Shugoshin, another tension sensor, also detects tensionless kinetochore-MT attachments and promotes the biorientation of sister kinetochores during mitosis. Unlike Aurora B^{Ipl1}, shugoshin cannot directly destabilize tensionless attachments but acts as an adaptor protein in recruiting Aurora B^{Ipl1}, thus promoting the biorientation of sister kinetochores. Though shugoshin plays an important role in the biorientation of chromosomes, several reports indicate that during mitosis, it is dispensable for the SAC activation (Indjeian et al., 2005, Vanoosthuyse et al., 2007, Sane et al., 2021). Shugoshin primarily localizes to centromeres, and phosphorylation of histone H2A at T120 in humans/S121 in yeasts by the SAC component Bub1 kinase plays a central role in targeting it to centromeres (Kawashima et al., 2010, Fernius and Hardwick, 2007).

Cryptococcus neoformans, a budding yeast, diverged from other ascomycete yeasts such as *S. cerevisiae* and *S. pombe* at least 500 MYA (Heitman, 2011). *C. neoformans* is an opportunistic pathogen belonging to Basidiomycota and is considered a critical priority fungal pathogen by the World Health Organization (WHO). Several species of *Cryptococcus* cause fungal meningitis (Kronstad et al., 2011), a fatal infection in immunocompromised patients. *C. neoformans* undergoes semi-open mitosis, and its nuclear division occurs in the daughter bud (Kozubowski et al., 2013). This is strikingly different as compared to relatively well-studied yeasts such as *S. cerevisiae* and *C. albicans* where the nuclear division occurs at the mother-daughter bud-neck junction (Sutradhar et al., 2015). The kinetochore architecture is significantly rewired *in C. neoformans,* where a linker protein bridgin presumably replaced the loss of most inner

125 kinetochore proteins (van Hooff et al., 2017, Sridhar et al., 2021). Moreover,
126 metazoan-like kinetochore maturation dynamics in *C. neoformans* during cell cycle
127 progression is distinctly different from most other budding yeast species (Kozubowski
128 et al., 2013). The cell cycle-associated dynamics of the centromere-kinetochore
129 complex in *C. neoformans* differ as well. Unlike other well-studied yeasts such as *S.*
130 *cerevisiae*, *S. pombe, and C. albicans,* where kinetochores are constitutively
131 clustered, the kinetochores in *C. neoformans* exhibit differential clustering dynamics,
132 where they are unclustered during interphase and cluster during mitosis.

133 Despite high medical importance, mechanisms monitoring kinetochore-MT
134 attachments have not been extensively studied in basidiomycete yeasts due to lack of
135 molecular tools. Studies to explore the roles of SAC components Bub1 (Madbub),
136 Mps1, and Mad1 in the checkpoint response using *C. neoformans* have just begun
137 (Leontiou et al., 2022, Aktar et al., 2024). Moreover, *C. neoformans* exhibits
138 aneuploidy-mediated fluconazole resistance (Sionov et al., 2010). Studying factors
139 that regulate kinetochore-MT attachments in this organism with rewired kinetochore
140 architecture and metazoan-like mitotic events might shed light on understanding
141 aneuploidy-driven drug resistance.

142 Here, we probed the role of an evolutionarily conserved protein, shugoshin, in *C.*
143 *neoformans* in monitoring the kinetochore-MT attachments during mitosis. We
144 propose that shugoshin performs this function by maintaining higher Aurora B^{Ipl1} and
145 lower PP1 levels at kinetochores during MT depolymerizing conditions. Unlike
146 ascomycete yeasts, shugoshin predominantly localizes to SPBs, along spindle MTs
147 and a minor pool at kinetochores during mitosis. Apart from the atypical localization,
148 we provide evidence that support that shugoshin targeting to its subcellular sites is not
149 dependent on the kinase activity of Bub1.

150 **Results**

151 **Shugoshin is required for efficient metaphase arrest in response to microtubule**
152 **depolymerizing drugs**

153 *SGO1* (FungiDB ORF ID: CNAG_05516) encodes the only form of shugoshin that is
154 expressed in *C. neoformans.* The putative 645-aa-long protein coded by *SGO1* has
155 an N-terminal coiled-coil domain and a C-terminal basic SGO motif (Fig 1A;
156 Supplementary Fig 1A and B). Multiple sequence alignment of amino acid sequences

157 revealed the presence of conserved residues required for PP2A binding
158 (Supplementary Fig 1B) (Xu et al., 2009). The SGO motif in *C. neoformans* shugoshin
159 also possesses a conserved lysine residue (K382) that is required for the binding of
160 shugoshin to phosphorylated histone H2A (Supplementary Fig 1B) (Kawashima et al.,
161 2010, Liu et al., 2013, Fernius and Hardwick, 2007). Previous studies reported that
162 shugoshin plays a role in ensuring proper kinetochore-MT attachments during mitosis
163 (see reviews (Gutierrez-Caballero et al., 2012, Marston, 2015)). Mutants affecting
164 kinetochore-MT interactions and proteins participating in the error correction
165 machinery and the SAC, are hypersensitive to MT depolymerizing drugs. To test if
166 Sgo1 contributes to the fidelity of mitotic chromosome segregation, we created *sgo1*
167 null mutants in *C. neoformans.* While Sgo1 was found to be dispensable for growth,
168 *sgo1* null mutant cells displayed sensitivity to a MT-depolymerizing drug,
169 thiabendazole (TBZ), similar to that of SAC mutant *mad2* (Fig 1B). These results
170 suggest that *sgo1Δ* mutant cells in the basidiomycete yeast *C. neoformans* have
171 phenotypes similar to those of ascomycete yeasts such as *Saccharomyces cerevisiae*,
172 *Schizosaccharomyces pombe* and *Candida albicans* (Indjeian et al., 2005, Kitajima et
173 al., 2004, Sane et al., 2021).

174 Next, we sought to test if enhanced sensitivity to the MT poison observed in *sgo1Δ*
175 mutant cells accentuate when combined with *mad2Δ* mutant. To test this, we created
176 *sgo1Δ mad2Δ* double mutants. Such double mutant cells exhibited synthetic lethality
177 in the presence of TBZ (Fig 1B), indicating that both Sgo1 and Mad2 are required for
178 an efficient SAC response in MT-depolymerizing conditions. This striking synthetic
179 lethality observed suggests that shugoshin is involved in functions such as
180 biorientation apart from promoting the SAC response, which is lost in *mad2Δ*. If
181 shugoshin is required for an efficient SAC response in *C. neoformans*, it is expected
182 that the *sgo1Δ* mutant, when combined with a kinetochore mutant, would enhance
183 sensitivities to TBZ. To explore this possibility, we used null mutant cells of a recently
184 reported basidiomycete-specific kinetochore linker protein bridgin (Bgi1). It has been
185 shown that *bgi1Δ* mutants are viable but exhibit gross chromosomal missegregation
186 (Sridhar et al., 2021). *bgi1Δ* mutants, combined with *mad2Δ*, displayed enhanced
187 sensitivity to TBZ compared to each of the single mutants alone (Sridhar et al., 2021).
188 The spotting assay indicated that *sgo1Δ bgi1Δ* double mutant cells are hypersensitive
189 to TBZ, similar to that of *mad2Δ bgi1Δ* (Supplementary Fig 2). Together, these results

190 reveal that shugoshin plays a role in proper kinetochore-MT interactions and/or
191 monitors defective attachments in response to spindle poison.

192 MT-depolymerizing drugs arrest wild-type cells at metaphase in the large-budded
193 stage with an undivided nucleus. Only when the defects are rectified will such cells
194 proceed to complete the cell division. To verify whether *sgo1Δ* mutants can induce
195 metaphase arrest when MTs are depolymerized, we performed a microscopy-based
196 assay to score for the cell cycle defects associated with *sgo1Δ* mutants by treating
197 cells with nocodazole (Fig 1C). Nocodazole-treated wild-type cells of *C. neoformans*
198 arrest at the large-budded stage with a visibly condensed chromatin mass (Fig 1C).
199 After 240 min of nocodazole treatment, >90% of wild-type cells were at the large-
200 budded stage with a condensed undivided nucleus (Fig 1C and Supplementary Fig
201 1C, D, and E). As expected, *mad2Δ,* a bonafide checkpoint-defective mutant, failed to
202 arrest cells at the large-budded stage (Fig 1C). In the *sgo1Δ* mutants, though we
203 initially observed an increase in the proportion of large-budded cells compared to
204 *mad2Δ* mutants, after 240 min post-nocodazole treatment, the large-budded cell
205 population significantly reduced (Fig 1C). Moreover, unlike wild-type, most large-
206 budded cells in *sgo1Δ* mutants had an uncondensed chromatin mass similar to *mad2Δ*
207 mutant cells (Supplementary Fig 1C, D, and E). In the case of *sgo1Δ mad2Δ* double
208 mutants, no significant differences in the proportion of large-budded cells were
209 observed when compared to *sgo1Δ* and *mad2Δ* single mutants (Fig 1C). Estimating
210 the ploidy content in nocodazole-treated cells using flow cytometry (Fig 1D) revealed
211 that wild-type cells arrested at 2n ploidy level. On the other hand, *mad2Δ* cells shifted
212 towards 4n, indicating a failure in arresting cells at metaphase and initiating the next
213 cell cycle events. Unlike *mad2Δ, sgo1Δ* cells displayed a ploidy content of 2n and 4n,
214 revealing the presence of cells that are delayed at metaphase and cells that have
215 initiated the next round of DNA replication. Similar results were also obtained in *sgo1Δ*
216 *mad2Δ* double mutants. Taken together, we show that shugoshin is required for an
217 efficient metaphase arrest in response to unattached kinetochores induced by MT-
218 depolymerizing drugs.

219

220

221 ***sgo1Δ* mutant cells fail to maintain the SAC component Bub1 at kinetochores in**
222 **response to prolonged microtubule depolymerization**

223 Why are *sgo1Δ* mutant cells not arrested when treated with an MT poison at
224 metaphase? It is possible that *sgo1Δ* mutant cells arrest at metaphase immediately
225 after being treated with the MT poison but were unable to maintain the arrest upon
226 prolonged exposure to the drug. To test this, we localized the SAC component Bub1
227 (Fig 2A) tagged with GFP in wild-type and *sgo1Δ* cells. A recent report (Leontiou et
228 al., 2022) suggested that Bub1 localizes to kinetochores in *C. neoformans* and plays
229 a central role in the SAC-mediated arrest. We synchronized *C. neoformans* cells by
230 arresting them at G2 using hypoxia (Ohkusu et al., 2004) and released them in the
231 presence of nocodazole (refer to Materials and Methods for further details) (Fig 2B).
232 Inducing physical hypoxia in *C. neoformans* results in 'unbudded' G2 arrest. These
233 G2-arrested cells enter mitosis synchronously when subjected to extensive aeration.
234 Upon release into nocodazole-containing media, wild-type cells accumulated at the
235 large-budded stage (Supplementary Fig 3) with GFP-Bub1 signals, which were
236 maintained until the end of the experiment (Fig 2C and D). In the case of *sgo1Δ* cells,
237 the proportion of Bub1-positive large-budded cells increased similarly to that of wild-
238 type until 120 min. However, beyond 200 min post-nocodazole treatment, a sudden
239 decline in the proportion of Bub1-positive large-budded cells was observed in the
240 mutant (Fig 2C and D). Studies in *S. pombe* have shown that the kinase-dead version
241 of Bub1 is checkpoint-proficient but fails to maintain prolonged SAC arrest (Fernius
242 and Hardwick, 2007)**.** A similar observation was reported in *C. neoformans*, where
243 *bub1-kd* mutant cells failed to sustain the arrest induced by nocodazole (Leontiou et
244 al., 2022)**.** To understand how checkpoint responses differ in *sgo1Δ* from *bub1-kd,* we
245 compared GFP-Bub1 localization dynamics in hypoxia-synchronized cells treated with
246 nocodazole (Fig 2C and D). Though neither *sgo1Δ* nor *bub1-kd* mutant cells could
247 maintain the arrest like the wild-type, *bub1-kd* cells were able to maintain the arrest
248 longer than *sgo1Δ* cells.

249 Moreover, Bub1 signal intensities in *sgo1Δ* and *bub1-kd* mutants were significantly
250 reduced compared to the wild-type (Fig 2E). To further support these observations,
251 we resorted to a single-cell microfluidics assay to quantitatively measure the
252 checkpoint response in individual cells treated with the MT poison (Fig 2F and G).
253 Using this system, we probed the GFP-Bub1 dynamics in wild-type, *sgo1Δ*, *bub1-kd,*

254 *sgo1Δ bub1-kd,* and *mad1Δ* mutant cells treated with nocodazole. Similar to the
255 results observed in the experiment performed with the synchronized cells, neither
256 *sgo1Δ* nor *bub1-kd* mutant cells could maintain checkpoint arrest like wild-type as
257 indicated by the lower mean kinetochore residence times of Bub1 (Fig 2G). Checkpoint
258 defective *mad1Δ* mutant cells were used as a control. The *sgo1Δ bub1-kd* double
259 mutant behaved like the *sgo1Δ* single mutant (Supplementary Fig 4A and B). These
260 results reveal that *sgo1Δ* cells, similar to *bub1-kd* cells, are proficient in checkpoint
261 activation but cannot maintain checkpoint signals during prolonged treatment with
262 nocodazole.

263 **Aurora B^{Ipl1} maintenance at kinetochores is affected in *sgo1Δ* mutants during**
264 **prolonged checkpoint arrest**

265 Shugoshin interacts with CPC proteins and helps in either the recruitment or
266 maintenance of CPC components at centromeres/kinetochores in *S. cerevisiae*, *S.*
267 *pombe* and humans (Hindriksen et al., 2017, Marston, 2015). Previously, we
268 established the role of Aurora B^{Ipl1} (a CPC component) in regulating nuclear division
269 during mitosis in *C. neoformans* (Varshney et al., 2019). Although it has been shown
270 that the entry of Aurora B^{Ipl1} into the nucleus coincides with the nuclear envelope
271 breakdown (NEBD), its localization to kinetochores remained unexplored. In this study,
272 we colocalized Aurora B^{Ipl1} with the inner kinetochore protein CENP-A at different cell
273 cycle stages (Supplementary Fig 5A). During G2, when kinetochores are clustered,
274 we could only detect weak signals of Aurora B^{Ipl1} that intensified as cells entered
275 metaphase. Apart from the kinetochore localization, we could also observe spindle-
276 like localization of Aurora B^{Ipl1} during anaphase (Supplementary Fig 5A). Upon
277 treatment with nocodazole, we observed colocalization of Aurora B^{Ipl1} with
278 kinetochores (Supplementary Fig 5B). To test whether kinetochore localization of
279 Aurora B^{Ipl1} is affected in *sgo1Δ* cells in *C. neoformans*, we synchronized both wild-
280 type and *sgo1Δ* mutant cells by inducing physical hypoxia followed by a release in
281 nocodazole-containing media (Fig 2B). We scored for Aurora B^{Ipl1}-3xGFP-positive
282 large-budded cells. In *sgo1Δ,* we observed a reduced proportion of Aurora B^{Ipl1}-
283 positive large-budded cells over time compared to wild-type (Fig 3A, B and
284 Supplementary Fig 6). Similar to the Bub1 levels in *sgo1Δ* mutant cells, a reduction in
285 the intensity of the Aurora B^{Ipl1} signals in the *sgo1Δ* cells was also observed compared

286 to the wild-type (Fig 3C). Taken together, we conclude that Sgo1 is required to
287 maintain Bub1 and Aurora B^{Ipl1} at kinetochores when MTs are depolymerized.

288 **Aurora B^{Ipl1} is required for the maintenance of Bub1 at kinetochores in response**
289 **to microtubule depolymerization**

290 Reduced Aurora B^{Ipl1} levels at kinetochores in *sgo1Δ* cells prompted us to test whether
291 the absence of Aurora B^{Ipl1} leads to failure of checkpoint arrest when treated with MT
292 depolymerizing agents. For conditional depletion of Aurora B^{Ipl1}, we placed the gene
293 under the *GAL7* promoter. We treated Aurora B^{Ipl1} –(over)expressed (permissive,
294 galactose media) and Aurora B^{Ipl1}-depleted (non-permissive, glucose media) cells with
295 nocodazole (Fig 3D). We assayed for large-budded cells with a condensed chromatin
296 mass as observed at metaphase. Cells (over)expressing Aurora B^{Ipl1} and treated with
297 nocodazole displayed a higher proportion of large bud arrested cells. In contrast, cells
298 depleted of Aurora B^{Ipl1} failed to arrest at the large-budded stage and exhibited an
299 increase in the proportion of tri-budded cells (Supplementary Fig 7A and B). Moreover,
300 approximately 50% of the large-budded cells displayed an uncondensed nuclear
301 mass, similar to what was observed in *mad2Δ* mutants (Supplementary Fig 7A and B).
302 These results suggest that Aurora B^{Ipl1} is required for an efficient metaphase arrest
303 when cells are treated with a spindle poison in *C. neoformans*.

304 To confirm these observations further, we examined GFP-Bub1 localization dynamics
305 in cells depleted of Aurora B^{Ipl1} and treated with nocodazole (Fig 3E). Aurora B^{Ipl1}-
306 depleted cells subjected to nocodazole treatment for 120 and 240 min were able to
307 load Bub1 initially but failed to maintain Bub1 at kinetochores upon prolonged
308 treatment with nocodazole (Fig 3E and F), similar to what was observed in *sgo1Δ*
309 mutant cells. We also noticed a significant reduction in the levels of Bub1 at
310 kinetochores in Aurora B^{Ipl1}-depleted cells similar to that of *sgo1Δ* mutants (Fig 3G).
311 These results reveal that Aurora B^{Ipl1} in *C. neoformans* helps maintain Bub1 at
312 kinetochores in the presence of nocodazole.

313 **Shugoshin antagonizes the recruitment of PP1 at kinetochores in response to**
314 **nocodazole treatment**

315 The kinase activity of Aurora B^{Ipl1} and the phosphatase activity of PP1 are antagonistic
316 at kinetochores (Tatchell et al., 2011, Lesage et al., 2011). We hypothesized that a
317 reduction in Aurora B^{Ipl1} levels leads to increased PP1 levels (Fig 4A), and higher PP1

318 levels may lead to the loss of Bub1 from kinetochores. We expressed PP1-GFP
319 (FungiDB ORF ID CNAG_03706; Supplementary Fig 8) in a CENP-A-mCherry
320 expressing strain (CNKB003). First, we studied the effect of *sgo1Δ* on PP1 localization
321 during nocodazole treatment (Fig 4B). Both wild-type and *sgo1Δ* cells exhibited GFP-
322 PP1 signals at kinetochores during the metaphase-arrested stage. Quantifying the
323 fluorescence signal intensity of PP1 revealed a marginal but significant increase in the
324 GFP-PP1 signal intensities at kinetochores in *sgo1Δ* compared to wild-type cells (Fig
325 4C). A similar result was observed when Aurora B^{Ipl1}-depleted cells were treated with
326 nocodazole (Fig 4D and E). The SAC can be silenced by dephosphorylation of MELT
327 repeats on $Knl1^{Spc105}$ with the help of PP1. As a result, checkpoint components are
328 removed from kinetochores (Pinsky et al., 2009, Rosenberg et al., 2011, Meadows et
329 al., 2011, Espeut et al., 2012, Vanoosthuyse and Hardwick, 2009, Nijenhuis et al.,
330 2014). Premature recruitment of PP1 to kinetochores is detrimental and leads to
331 chromosome mis-segregation (Roy et al., 2019). Based on the results described
332 above, we propose that the increase in PP1 levels at kinetochores leads to the loss of
333 Bub1 signals in the absence of shugoshin or Aurora B^{Ipl1}, which interferes with the
334 SAC maintenance in MT depolymerizing conditions.

335 **The tension-sensing function of shugoshin is conserved in *C. neoformans***

336 Shugoshin senses tensionless attachments by recruiting several factors that play a
337 role in correcting tensionless attachments (Marston, 2015). Cohesin is a molecular
338 glue that holds two sister chromatids together during mitosis until metaphase. Cohesin
339 plays an essential role in generating tension that resists the pulling force of MTs, aiding
340 high-fidelity chromosome segregation (Guacci et al., 1997, Michaelis et al., 1997).
341 Loss of cohesion at centromeres results in tensionless kinetochore-MT attachments.
342 To test if Sgo1 in *C. neoformans* detects tensionless attachments, we depleted one of
343 the cohesin subunits, Scc1/Mcd1/Rad21, by placing it under the *GAL7* promoter both
344 in the wild-type and *sgo1Δ* mutant cells. *C. neoformans* Scc1 (FungiDB ORF ID
345 CNAG_01023) harbors N- and C-terminal Scc1 domains (Supplementary Fig 9A and
346 B). We show that like *S. cerevisiae* and *S. pombe, SCC1* in *C. neoformans* is essential
347 for viability (Supplementary Fig 9C). Upon depletion of Scc1, a high proportion of wild-
348 type cells are arrested at the large-budded stage (Supplementary Fig 9D, E, and F).
349 In contrast, the *sgo1Δ* mutants depleted of Scc1 did not show such an increase in the

350 proportion of large-budded cells, indicating that shugoshin plays a role in detecting
351 tensionless kinetochore-MT attachments and delays the cell cycle progression.

352 **Shugoshin is enriched at the spindle pole bodies (SPBs) and spindle during**
353 **mitosis**

354 Thus far, we reveal an unknown role of Sgo1 in maintaining Bub1 through the balance
355 of Aurora B^{Ipl1} and PP1 at kinetochores in *C. neoformans*. Next, we examined the cell
356 cycle localization dynamics of Sgo1 in *C. neoformans*. Shugoshin localizes to the
357 kinetochore during cell division in most species studied (Marston, 2015)
358 (Supplementary Fig S11). To find the sub-cellular localization of Sgo1, we expressed
359 GFP-Sgo1 from its native locus in the CENP-A-mCherry tagged strain. We
360 synchronized the cells using hypoxia to examine the cell cycle stage-specific
361 localization of Sgo1. No signals of Sgo1 could be observed during most of the
362 interphase. In G2, where all centromeres cluster as a single punctum (Kozubowski et
363 al., 2013, Sridhar et al., 2021), we observed Sgo1 signals near clustered centromeres
364 (Fig 5A). Upon entry into mitosis, Sgo1 appeared as two distinct puncta that flanked
365 the bar-like signals of CENP-A. Apart from the punctate signals of Sgo1, we observed
366 weak signals along the pole-to-pole axis during metaphase and anaphase that
367 resembled spindle-like localization. To examine whether Sgo1 localizes to spindle pole
368 bodies (SPBs), we expressed Tub4-mCherry (γ-tubulin) in the GFP-Sgo1 expressing
369 strain. GFP-Sgo1 signals colocalized with SPBs during G2 and mitotic stages (Fig 5B),
370 indicating that Sgo1 localizes predominantly to SPBs during the mitosis in *C.*
371 *neoformans*.

372 To test if the spindle-like localization during mitosis depends on the spindle MT
373 integrity, we arrested cells at metaphase using two methods. First, we used
374 nocodazole to depolymerize MTs that activate the SAC and arrest cells at metaphase.
375 Second, we depleted Cdc20, an anaphase-promoting complex/cyclosome (APC/C)
376 component. Depletion or inactivation of Cdc20 leads to metaphase arrest in *S.*
377 *cerevisiae* (Hwang et al., 1998). Upon treating *C. neoformans* cells with nocodazole,
378 we observed that Sgo1 colocalized with the SPB (Fig 5C). On the other hand, depletion
379 of Cdc20 by placing it under the galactose regulatable promoter (*GAL7*) resulted in
380 metaphase arrest, and the spindle-like localization of shugoshin along the pole-to-pole

381 axis was maintained (Fig 5D). These observations led us to conclude that the spindle-
382 like localization of Sgo1 requires intact MTs during mitosis.

383 **The kinase activity of Bub1 is dispensable for the function and localization of**
384 **shugoshin during mitosis in *C. neoformans***

385 Studies from several yeast species and humans reveal that Bub1 is one of the major
386 factors that recruit shugoshin to kinetochores. Although Bub1 plays a critical role,
387 several other proteins such as cohesin, heterochromatin protein (HP1), CPC, and
388 CENP-A also contribute to the targeting of shugoshin to kinetochores, see review
389 (Marston, 2015) (Fig 6A). In the present study, to test if the Bub1 kinase activity
390 required for shugoshin's function is evolutionarily conserved in *C. neoformans*, we
391 utilized the kinase-dead (*bub1-kd*) mutant of Bub1. *In vitro* assays reported earlier
392 (Leontiou et al., 2022) revealed that Bub1 could phosphorylate the reconstituted
393 human H2A containing nucleosomes, and kinase-dead mutants of Bub1 fail to
394 phosphorylate. We performed a genetic interaction assay by scoring the TBZ
395 sensitivity of *sgo1Δ*, *bub1-kd*, and *sgo1Δ bub1-kd* mutants (Fig 6B). If both Sgo1 and
396 Bub1 kinase activity function in the same pathway in *C. neoformans*, one would expect
397 little to no change in the sensitivity of double mutants compared to either of the single
398 mutants, *sgo1Δ* and *bub1-kd*. By dilution spotting assay, we observed that the *bub1-*
399 *kd sgo1Δ* double mutant cells behaved like that of the *sgo1Δ* mutant (Fig 6B).
400 Moreover, the sensitivity of *sgo1Δ* mutant cells to TBZ is higher than that of *bub1-kd*
401 mutant. There are two possibilities for the above observations. First, the enhanced
402 sensitivity of the *sgo1Δ* mutant could be due to the additional functions of the
403 shugoshin that do not rely on the kinase activity of Bub1. Second, the kinase activity
404 of Bub1 does not play a significant role in dictating the kinetochore/kinetochore
405 proximal localization of Sgo1. To test these possibilities, we have localized GFP-Sgo1
406 and performed a genetic interaction assay using mutants known to disrupt Bub1
407 kinase-mediated targeting of shugoshin in other species.

408 The lysine residue K382 in Sgo1 in *C. neoformans* corresponds to the lysine K492 in
409 Sgo1 in humans (Supplementary Fig 1B). This residue is known to play a role in
410 binding to phosphorylated H2A (Kawashima et al., 2010, Liu et al., 2013). A mutation
411 in the lysine residue of shugoshin in fission yeast (K298) or humans (K492) results in
412 the loss of kinetochore localization of shugoshin in mitosis (Liu et al., 2013,

413 Kawashima et al., 2010). Similarly, mutating the S121 (budding/fission yeast) or T121
414 (humans) residue of histone H2A also abrogates the kinetochore localization of the
415 shugoshin (Liu et al., 2013, Kawashima et al., 2010). To test the role of these
416 conserved residues in *C. neoformans*, we mutated K382 in Sgo1 (Supplementary Fig
417 1B) and T121 in H2A to alanine (Supplementary Fig 10A). The plasmid constructs
418 harboring either wild-type *SGO1* or a *sgo1-K382A* allele were integrated into the *SAFE*
419 *HAVEN* locus (chromosome 1) (Arras et al., 2015) of the *sgo1Δ* strain. An overlap
420 PCR construct harboring the *h2a-T121A* mutation was transformed into a strain
421 expressing GFP-SGO1 and mCherry-CENP-A. If the kinase activity of Bub1 is indeed
422 dispensable for shugoshin's checkpoint function during mitosis, the strain carrying
423 the *GFP-sgo1-K382A* allele would rescue the sensitivity to spindle poisons. Similarly,
424 strain harboring the *h2a-T121A* allele would not show any sensitivity. Spotting assays
425 on TBZ plates revealed that both sgo1-*K382A* and *h2a-T121A* mutants behaved like
426 wild-type cells (Fig 6C). To further confirm these results, we localized Sgo1 in the
427 above-mentioned mutant strains. Since Sgo1 exhibits both SPB and spindle-like
428 localization during metaphase, we have obtained metaphase cells using hypoxia or
429 thiabendazole arrest followed by release to score for the localization (refer to materials
430 and methods for details). In both budding and fission yeasts, *bub1-kd*, *h2a-SA,* and
431 *sgo-KA* mutants abolish kinetochore localization of shugoshin (Kawashima et al.,
432 2010). In sharp contrast, we observed that *sgo1-K382A, h2a-T121A,* and *bub1-kd*
433 mutants in *C. neoformans* did not abolish the SPB or spindle-like localization of Sgo1
434 during metaphase (Fig 6D and E). Sgo1 levels were unaffected in the above mutants
435 (Supplementary Fig 10B). These results confirm that the kinase activity of Bub1 is
436 dispensable for the recruitment of shugoshin and its SAC maintenance function in *C.*
437 *neoformans.*

438 In *C. neoformans,* Sgo1 predominantly localizes to SPBs and the spindle during
439 metaphase. The metaphase spindle localization of Sgo1 overlaps with CENP-A (Fig
440 5A). To probe if the kinetochores at the metaphase stage bind to Sgo1, we performed
441 chromatin immunoprecipitation (ChIP) assay in Scc1-depleted cells (Fig 6F, top
442 panel). Microscopy analysis of Scc1-depleted cells showed both SPB and spindle-like
443 localization of Sgo1 (Fig 6F, bottom panel) as observed previously (Fig 5). ChIP assay
444 indicates that there is only a minor enrichment of Sgo1 at centromeres in *C.*
445 *neoformans* (Fig 6G), suggesting that the association of Sgo1 with centromeres could

446 be transient in nature and/or only a minor pool of Sgo1 is associated with kinetochores
447 and the majority could be along the spindle.

448 **Discussion**

449 In this study, we characterized the mitotic functions of shugoshin in *C. neoformans*.
450 The only form of shugoshin, coded by *SGO1*, predominantly localizes to SPBs and
451 along the mitotic spindle in *C. neoformans*. In response to prolonged MT
452 depolymerization, Sgo1 maintains adequate Aurora B^{Ipl1} levels at kinetochores to
453 antagonize premature phosphatase action of PP1 at kinetochores. Thus, by regulating
454 an optimum balance of the protein kinase Aurora B^{Ipl1} and the protein phosphatase
455 PP1, shugoshin retains checkpoint responses until errors are corrected. Together, we
456 report that Sgo1 regulates PP1 levels at kinetochores in response to microtubule
457 depolymerization. We also demonstrated that the checkpoint maintenance function of
458 Sgo1 is independent of the evolutionarily conserved Bub1 kinase activity-mediated
459 targeting of Sgo1 to centromeres/kinetochores.

460 Sgo1 is not required to activate the SAC; rather, it helps prolong the SAC response by
461 maintaining the levels of Bub1 at kinetochores in *C. neoformans*. Similarly, Aurora B^{Ipl1}
462 also helps in the maintenance of Bub1 levels at kinetochores in response to MT
463 depolymerization conditions. Studies in *S. cerevisiae*, *S. pombe*, flies, and humans
464 reveal that shugoshin interacts with the chromosome passenger complex (CPC) and
465 is required for either recruitment or maintenance of Aurora B^{Ipl1} to correct tensionless
466 kinetochore attachments (Hindriksen et al., 2017, Marston, 2015). We show that apart
467 from maintaining Bub1 levels at kinetochores, Sgo1 is also required to maintain Aurora
468 B^{Ipl1} levels when treated with nocodazole. Microfluidics and time course assays (Fig
469 2D, F, and 3B) indicate that *sgo1Δ* mutants can load Bub1 or Aurora B^{Ipl1} at
470 kinetochores albeit to a lesser level, but over time, the localization of these proteins is
471 lost in the large-budded cells. This suggests that the loss of Bub1 or Aurora B^{Ipl1} from
472 kinetochores leads to failure in SAC maintenance in *sgo1Δ* cells during MT
473 depolymerizing conditions. We hypothesize that Sgo1 regulates the SAC function
474 through Aurora B^{Ipl1} in two ways that may not necessarily be mutually exclusive: a) by
475 maintaining high Aurora B^{Ipl1} activity at kinetochores, thereby preventing the action of
476 PP1 in terminating SAC signals, and b) by regulating Mps1 and Bub3/Bub1 (Saurin et
477 al., 2011, Roy et al., 2022, Audett et al., 2022) at kinetochores, thereby modulating the

478 SAC response. The fact that we observe an increase in the levels of PP1 at
479 kinetochores in the reduced levels of Aurora B^{Ipl1} indicates that Sgo1, more likely, acts
480 through Aurora B^{Ipl1} to antagonize the activity of PP1 at kinetochores thereby
481 preventing the premature SAC termination.

482 The fact that Sgo1 is not required for the SAC activation but for the maintenance of
483 the SAC response via maintaining a balance between Aurora B^{Ipl1}-PP1 at kinetochores
484 also explains why *sgo1Δ mad2Δ* double mutants are synthetic lethal in the presence
485 of MT depolymerizing drugs. The observed synergy indicates that both Sgo1 and
486 Mad2 act in different pathways, where Sgo1 may play other roles such as biorientation
487 of chromosomes that function (i) via the Aurora B^{Ipl1}-PP1-Bub1 axis; (ii) by recruiting
488 condensin (Verzijlbergen et al., 2014, Peplowska et al., 2014) to the centromeres
489 which biases sister kinetochores to bi-orient by affecting the kinetochore geometry;
490 (iii) by maintaining the centromeric cohesion to prevent premature separation of sister
491 chromatids, see review (Marston, 2015).

492 The mechanism of recruitment of shugoshin to kinetochores is a stratified process as
493 it involves several proteins. Among these, Bub1 plays a critical role in targeting
494 shugoshin to kinetochores in *S. cerevisiae*, *S. pombe*, *Xenopus laevis,* and humans
495 (Liu et al., 2013, Kawashima et al., 2010, Boyarchuk et al., 2007) (Fig 6A). In humans,
496 it has been reported that Cdk1-mediated phosphorylation of shugoshin promotes its
497 interaction with cohesin and targeting to inner centromeres (Liu et al., 2013). Similarly,
498 in *S. cerevisiae* (Kiburz et al., 2005) and *S. pombe* (Kitajima et al., 2004) cohesins are
499 known to interact with shugoshin and this association in *S. cerevisiae* promotes the
500 recruitment of shugoshin to pericentromeric regions in mitosis (Verzijlbergen et al.,
501 2014, Kiburz et al., 2005). Apart from cohesins, it has been shown that a
502 heterochromatin protein, HP1 promotes centromeric recruitment of shugoshin in *S.*
503 *pombe* (Yamagishi et al., 2008). It has also been reported that shugoshin and the CPC
504 complex mutually influence each other's localization at centromeres. In *Drosophila*,
505 the phosphorylation of MEI-S332 (shugoshin) by Aurora B^{Ipl1} promotes its centromere
506 localization (Nogueira et al., 2014, Resnick et al., 2006). Studies have also implicated
507 the role of CENP-A and H3 nucleosomes in targeting shugoshin to centromeres as
508 well (Wu et al., 2024, Mishra et al., 2018, Luo et al., 2016, Ng et al., 2013, Luo et al.,
509 2010). Intriguingly, in C. neoformans, the checkpoint maintenance function of Sgo1 is
510 not mediated through the Bub1-pH2A axis, as disruption of this pathway did not

511 abolish the Sgo1 localization or the SAC maintenance function. This suggests that
512 Bub1 is not a major player in recruiting CnSgo1 unlike the other species studied. We
513 speculate that the Bub1 independent recruitment of CnSgo1 could be due to the non-
514 canonical localization of the major pool of shugoshin at SPBs and along the mitotic
515 spindle.

516 Altogether, this study illustrates the functional diversity of an evolutionarily conserved
517 protein, shugoshin. A spatio-temporal balance of kinase and phosphatase activity is
518 crucial for proper kinetochore-MT attachments and SAC signaling. Sgo1 monitors the
519 kinetochore-MT attachment state in mitosis by balancing Aurora B^{Ipl1} and PP1 levels
520 at kinetochores. Based on the ChIP data, it is possible that there could be a transient
521 and/or a minor pool of shugoshin associated with the kinetochores or kinetochore
522 proximal regions. SPBs and spindle microtubules, along with other proteins such as
523 HP1, CPC, CENP-A, and histone H3, might promote the kinetochore proximal
524 association of Sgo1 in *C. neoformans*. This kinetochore proximal localization of
525 shugoshin may not primarily rely on Bub1 kinase function. It is also possible that CPC
526 or the activity of polo-like kinase (Cdc5/PLK1) as reported in humans (Wang et al.,
527 2008) may also play a role in targeting Sgo1 to SPBs. Further investigation is needed
528 to confirm the importance of SPBs/microtubules in regulating the function of Sgo1 in
529 this organism of high medical importance.

530 **Materials and Methods**

531 **Strains and media growth conditions**

532 *C. neoformans* cultures were grown and maintained on YPD (1% yeast extract, 2%
533 peptone, and 2% dextrose) and YPG (1% yeast extract, 2% peptone, and 2%
534 galactose) media at 30°C unless specified. YPD+1M sorbitol or YPG+1M sorbitol
535 plates were used for transformation. For the selection of transformants, 100 µg/mL of
536 nourseothricin (NAT, clonNAT, Werner BioAgents), 180 µg/mL neomycin (G-418,
537 Sigma-Aldrich), and 220 µg/mL of hygromycin (HiMedia) were used.

538 **Biolistic transformation**

539 The biolistic transformation was done based on a previously described method
540 (Davidson et al., 2000). Approximately 5 mL of *C. neoformans* culture was grown
541 overnight, centrifuged at 4,000 rpm for 5 min, and resuspended in 300 µL sterile dH_2O.
542 Around 300 µL of cell suspension was spread on the YPD+1M sorbitol plate and dried.
543 Gold micro-carrier beads (0.6 µm) coated with 2-5 µg of DNA were prepared, and 10
544 µL of 2.5 M $CaCl_2$, 2 µL of 1M spermidine free base (Sigma-Aldrich) were added. The
545 mixture was vortexed for 30 s, incubated for 10 min at room temperature, centrifuged,
546 washed with 500 µL of 100% ethanol, and resuspended in 10 µL of 100% ethanol. The
547 solution was placed on a micro-carrier disk and allowed to dry. Dried disks were placed
548 in the biolistic transformation apparatus (Biolistic® PDS-1000/He Particle Delivery
549 System). Helium gas pressure of approximately 1300 psi under a vacuum of a
550 minimum of 25 inches of Hg was generated to bombard the cells with micro-carrier
551 beads. The cells were incubated for 5-6 h in YPD+1M sorbitol medium at 30°C. Cells
552 were then plated on YPD+NAT/NEO/HYG selection plate and incubated at 30°C for
553 3-4 days.

554 **Strains and plasmids**

555 Lists of strains, plasmids, and primers used in this study are provided in Tables S1-
556 S3. The construction of *C. neoformans* strains and plasmids is detailed below.

557 ***GFP-SGO1* strains**

558 The fluorescent fusion protein of shugoshin was generated by cloning the 1200 bp
559 homology region and the *SGO1* promoter into the pVY7 plasmid containing the GFP

560 and NAT sequences. GFP was tagged to the N-terminal region of the *SGO1* gene.
561 The primers used for generating the clone are listed in Table S3. The 1200 bp
562 homology region and a 500 bp *SGO1* promoter region were amplified from the *SGO1*
563 gene using *C. neoformans* (H99) genomic DNA. The individual PCR fragments were
564 gel purified. The amplified regions were cloned using BamHI, SacI, and NcoI sites.
565 The final clone was linearized using HindIII and transformed into H99 and CNVY101.
566 The transformants obtained were confirmed by PCR.

567 ***sgo1Δ* strains**

568 An overlap PCR strategy was used to delete *SGO1* gene in the desired strains. Around
569 1000 bp region upstream to the start codon (ATG) and 1000 bp downstream region of
570 the stop codon of the *SGO1* ORF was amplified using *C. neoformans* (H99) genomic
571 DNA. The *NEO* resistance marker fragment was amplified from the pLK25 plasmid
572 (Table S2). The individual PCR fragments were gel purified. Using these individual
573 PCR amplified fragments, a final overlap cassette of ~3800 bp was constructed using
574 primers (Table S3). The final cassette was used to transform *C. neoformans*. The
575 transformants obtained were confirmed by PCR. To delete the *SGO1* gene in different
576 strain backgrounds, the *NEO* marker was swapped with either *NAT* or *HygB* genes
577 amplified from the pVY7 and pSH7G plasmids (Table S2) using the same set of
578 primers. The *sgo1Δ* cassette was used to transform H99, CNVY108, SHR741,
579 SHR830, IL102, IL143, CNKB003 and CNSD190 strains. The transformants obtained
580 were screened by PCR.

581 ***TUB4-mCherry* strain**

582 An overlap PCR strategy was used to tag Tub4 with mCherry at C-terminus. Primers
583 used for overlap cassette construction are listed in Table S3. Around 1000 bp region
584 upstream to the stop codon (without including the stop codon) and 1000 bp 3' UTR
585 region after the stop codon was amplified from the *TUB4* ORF using *C. neoformans*
586 (H99) genomic DNA. The mCherry sequence with antibiotic resistance marker NEO
587 was amplified from the pLK25 plasmid (Table S2). The individual PCR fragments were
588 gel purified. A final overlap cassette of ~4500 bp was constructed using individual PCR
589 fragments. The final cassette was transformed into CNSD127 strain. The
590 transformants obtained were confirmed by PCR.

591

592 ***GAL7-3xFLAG* tagged *SCC1*, *AURORA B^{IPL1}*, *CDC20* strains**

593 To place the desired gene under regulatable *GAL7p* along with an N-terminal 3xFLAG
594 sequence, an overlap PCR strategy was used. Around 1000 bp regions upstream (US)
595 and downstream (DS) of the start codon (ATG) of the ORFs of interest were amplified
596 using *C. neoformans* (H99) genomic DNA. *GAL7* promoter with *HygB* resistance gene
597 was amplified from pSH7G plasmid, and the 3xFLAG sequence was introduced using
598 a primer (Table S3). The individual PCR fragments were gel purified. A final overlap
599 cassette was assembled using the individual purified fragments. The cassettes
600 generated were transformed into *C. neoformans* and the positive transformants were
601 confirmed by PCR. The 3xFLAG tagged conditional mutants of *SCC1*, *AURORA B^{IPL1}*,
602 and *CDC20* generated using the strategy mentioned above are listed in Table S1.

603 ***AURORA B^{IPL1}-3xGFP mCherry-CENP-A* strain**

604 The H99 strain expressing Aurk B^{Ipl1}-3xGFP and mCherry-CENP-A was generated by
605 the random integration of the plasmid pLKB71 (Table S2). The mCherry-CENP-A
606 construct is expressed using the *H3* promoter. To create the strain, the plasmid
607 backbone of pLKB71 was digested with HindIII and transformed into CNNV113, and
608 the transformants were selected on the YPD-agar plate containing hygromycin
609 selection. The colonies obtained were screened using a Zeiss Axio Observer 7
610 widefield microscope for the transformants positive for the mCherry-CENP-A signal.

611 ***GFP-PP1 mCherry-CENP-A* strain**

612 The N-terminal GFP fusion protein of PP1 was generated by cloning around 1000 bp
613 homology region and PP1 promoter into the pVY7 plasmid containing GFP and NAT
614 sequences. Around 955 bp PP1 promoter region and 1000 bp PP1 homology region
615 were amplified from PP1 ORF using *C. neoformans* (H99) genomic DNA. The PCR
616 amplicons were gel purified. The digested amplicons of promoter and homology region
617 were cloned into pVY7 using SacI, NcoI, and SpeI sites, respectively. The final clone
618 was linearized using BglII and transformed into the CNVY101 strain, and the positive
619 transformants were confirmed by PCR.

620

621

622 ***GFP-sgo1-K382A-SH1*, *GFP-SGO1-SH1* and *GFP-sgo1-K382A-SH1 mCherry-***
623 ***CENP-A* strains**

624 The N-terminal GFP fusion protein of wild-type and mutant (K382A) allele of *SGO1*
625 was generated by cloning *SGO1* promoter, *SGO1* ORF, and 3'UTR into the pSD29
626 plasmid (Table S2) containing the GFP, HygB and *SAFE HAVEN* sequences. Around
627 2340 bp of *SGO1* ORF 315 bp of *SGO1* promoter, and 436 bp of 3'UTR were amplified
628 from the *SGO1* gene using *C. neoformans* (H99) genomic DNA. The K382A mutation
629 in the *SGO1* ORF was introduced using overlap PCR. The primers used are listed in
630 Table S3. The individual PCR fragments were gel purified. The purified fragments of
631 the *SGO1* promoter, *SGO1* ORF, and 3'UTR were cloned sequentially using SpeI,
632 BamHI, HpaI, NheI, and ApaI sites. The final clone was linearized using XcmI and
633 transformed into CNSD113. The transformants obtained were confirmed by PCR, and
634 Sanger sequencing was performed to confirm the presence of the *K382A* mutation.
635 The strain harbouring *GFP-sgo1-K382A* allele at *SAFE HAVEN* locus was transformed
636 with mCherry-CENP-A-NAT plasmid linearized using BglII and the positive
637 transformants were confirmed by microscopy.

638 ***h2a-T121A GFP-SGO1 mCherry-CENP-A strain***

639 A 1503 bp fragment of H2A ORF and 3' UTR was amplified by PCR using *C.*
640 *neoformans* (H99) genomic DNA and the T121A mutation was introduced into the
641 1503 bp fragment using overlap PCR strategy. A second fragment containing a
642 Hygromycin marker was amplified from pSH7G. The homology region downstream of
643 H2A 3' UTR was amplified by PCR using *C. neoformans* (H99) genomic DNA. The
644 primers used for generating the construct are listed in Table S3. The three PCR
645 fragments were subsequently fused by overlap PCR. The final overlap product was
646 used to transform the CNSD125 strain using the biolistic transformation method, and
647 the transformants obtained were confirmed by PCR, and Sanger sequencing was
648 performed to confirm the presence of mutation within the gene.

649 ***bub1-kd 3xFLAG GFP-SGO1 mCherry-CENP-A* strain**

650 The 3xFLAG-tagged bub1-kd cassette was generated by cloning the 1200 bp
651 homology region of BUB1 ORF harboring point mutations into the pSH7G plasmid
652 containing the HYG sequences. The primers used for generating the clone are listed
653 in Table S3. The 1200 bp homology region was amplified from the *bub1-kd* allele using

654 genomic DNA obtained from the IL143 (*GFP-bub1-kd*) strain. The individual PCR
655 fragments were gel purified. The amplified regions were cloned using SpeI and KpnI
656 sites. The final clone was linearized using ApaI and transformed into CNSD125
657 background using the biolistic transformation method. The transformants obtained
658 were confirmed by PCR.

659 **Thiabendazole sensitivity assay**

660 For assaying sensitivity to thiabendazole, the $O.D_{600}$ values of overnight cultures of
661 wild-type and mutants used in this study were estimated, and serial dilutions starting
662 from 10^5 cells to 10^1 cells were spotted on YPD-agar, DMF (Dimethyl Formamide);
663 control, and YPD-agar plates with different concentrations of thiabendazole (2.0, 2.5,
664 3.0 and 4.0 µg/mL). The plates were incubated at 30°C for 24 to 48 h and imaged
665 using a Bio-Rad chemidoc imaging system.

666 **Synchronization of *C. neoformans* by inducing physical hypoxia**

667 For the synchronization of *C. neoformans* cells, we have used a protocol developed
668 by Ohkusu et al., (Ohkusu et al., 2004) which utilizes a two-step protocol for the
669 synchronization. *C. neoformans* cells, when grown in hypoxia conditions, result in
670 unbudded G2 arrest, and cells release synchronously once shifted to extensive
671 aeration conditions. Hypoxia synchrony is a two-step process. First, cells were grown
672 at moderate aeration to 4.0 $O.D_{600}$/mL in a 250 mL flask (Borosil Erlenmeyer flask with
673 a screw cap was used for this experiment) with 50 mL of 1% YPD at 100 rpm, 30 °C.
674 In the second step, the culture was diluted 1.5 times with fresh 1% YPD (final volume
675 of 125 mL) and then incubated further for 5 h. The second step induces physical
676 hypoxia, and at the end of the incubation, most cells get arrested at the unbudded G2
677 stage.

678 For the synchronization experiments, we used an overnight culture grown in 1% YPD
679 to inoculate the secondary culture at 0.1 $O.D_{600}$/mL in 1% YPD and grown to 1
680 $O.D_{600}$/mL at 180 rpm, 30°C. This log phase culture was used for hypoxia synchrony,
681 as mentioned above. The percentage of cells in the unbudded G2 stage was confirmed
682 using a microscope. The culture was diluted to 1 $O.D_{600}$/mL using fresh media,
683 transferred to a sterile falcon or conical flask with appropriate culture volumes, and
684 released under extensive aeration conditions (180 rpm, 30°C).

685 **GFP-Bub1 and Aurora B^{Ipl1}-3xGFP retention assay**

686 To study the localization dynamics of GFP-Bub1 and Aur B^{Ipl1}-3xGFP in response to
687 nocodazole treatment, wild-type, and *sgo1Δ* mutants were subjected to hypoxia
688 synchrony, and the cells were released into 1% YPD media containing 1 µg/mL
689 nocodazole. Time points were collected every 40 minutes until 280 min. The cells
690 collected were imaged using a Zeiss Axio Observer 7 widefield microscope. A circular
691 ROI of 12*12 or 6*6 pixels was used to measure the signal intensities. The presence
692 or absence of GFP-Bub1 signals was scored manually. The cells that show bright
693 punctate localization of Bub1 above the cell background were considered positive for
694 Bub1.

695 **Imaging GFP-Sgo1 localization in *mCherry-CENP-A* and *TUB4-mCherry* strains**

696 For imaging GFP-Sgo1 colocalization with CENP-A- and Tub4-mCherry tagged
697 proteins, we synchronized cells using physical hypoxia. Cells were released into 1%
698 YPD and collected every 10 min starting from 30 to 90 min. Cells were imaged using
699 a Zeiss Axio Observer 7 widefield microscope.

700 **Cell cycle synchronization using thiabendazole (TBZ)**

701 In order to obtain metaphase cells, the overnight-grown culture of *Cryptococcus* was
702 inoculated at 0.2 $O.D_{600}$/mL and grown to log phase. The log phase culture was treated
703 with 10 µg/mL thiabendazole for 2 h. The cells arrested at G2/M were washed twice
704 with 2% YPD and released into fresh pre-warmed 2% YPD by incubating at 30°C, 180
705 RPM for 2 min. The cells were harvested by spinning at 5000 RPM for 30 seconds,
706 washed twice with sterile water, and imaged using a Zeiss Axio Observer 7 widefield
707 microscope.

708 **Line scan analysis of GFP-Sgo1 signal at metaphase stage.**

709 For measuring the fluorescent intensity of Sgo1 at metaphase in wild-type and the
710 *bub1-kd*, *h2a-T121A,* and *sgo1-K382A* strains, a line of 2-pixel thickness and a length
711 of approximately 3.4 µm was drawn using a line tool available in Fiji (Schindelin et al.,
712 2012). A single Z-plane containing both SPB and spindle signals was considered for
713 intensity measurement. The fluorescence intensity values along the line were
714 measured using the plot profile function. The intensity values of the GFP signal

715 obtained from different cells were averaged and divided by the average background
716 of the cells. The normalized intensity values were plotted using GraphPad Prism.

717 **Budding index calculation**

718 The proportion of unbudded, small-budded, and large-budded cells was calculated
719 based on the budding index (diameter of daughter cell/diameter of mother cell). The
720 diameters of both mother and daughter cells were calculated along the mother-
721 daughter axis using the line tool in Fiji (Schindelin et al., 2012).

722 **Fluorescence microscopy**

723 For widefield microscopy, Zeiss Axio Observer 7 equipped with 100x Plan Apochromat
724 1.4 NA objective, Colibri 7 LED light source, motorized XYZ stage and PCO.edge 4.2
725 sCMOS camera was used. Images were acquired at 2x2 or 4x4 binning. Zen blue
726 edition (2.3) software was used for controlling the microscope components and
727 acquisition. For imaging, cells grown in culture media were washed twice with
728 autoclaved dH_2O and resuspended in water. The cell suspension was placed on
729 microscope cover glass and imaged.

730 ***Time-lapse microfluidic assays***

731 The utility of microfluidics for single-cell analysis in *Cryptococcus* was demonstrated
732 previously in studies of aging (Orner et al., 2019). We used the Alcatras cell traps
733 (Crane et al., 2014) incorporated into devices allowing for use with multiple strains
734 (Granados et al., 2018, Granados et al., 2017). Devices were moulded in
735 polydimethylsiloxane (PDMS) from a SU8-patterned wafer with an increased thickness
736 of 7 µm to accommodate the larger size of *C neoformans* cells compared to *S*
737 *cerevisiae* (manufactured by Micro-resist, Berlin, design available on request).
738 Imaging chambers for individual strains were isolated by arrays of PDMS pillars
739 separated by 2 µm gaps. This prevents the intermixing of strains while cells experience
740 identical media conditions. Before use, the devices were filled with synthetic complete
741 (SC) media, supplemented with 0.2 g/L glucose, and containing 0.05% w/v bovine
742 serum albumin (Sigma) to reduce cell-cell and cell-PDMS adhesion. Cells pre-grown
743 to logarithmic phase in the same media (lacking the BSA) were injected into the device.
744 An EZ flow system (Fluigent) delivered media at 10 µl per minute to the flow chambers
745 and performed the switch to media containing nocodazole after 5 hours. This media

746 also contained Cy5 dye to allow monitoring of the timing of the media switch. Image
747 stacks were captured at 2-minute intervals at 4 stage positions for each strain, using
748 a Nikon TiE epifluorescence microscope with a 60x oil-immersion objective (NA 1.4),
749 a Prime95b sCMOS camera (Teledyne Photometrics) and OptoLED illumination
750 (Cairn Research). Image stacks had 5 Z-sections, separated by 0.6 µm, captured
751 using a piezo lens positioning motor (Pi).

752 ***Time-lapse* microfluidic assay image processing and analysis**

753 Time-lapse assays were performed as described (Leontiou et al., 2022). Cell outlines
754 were segmented using the baby algorithm (Pietsch et al., 2023). To quantify the
755 kinetochore retention time of GFP-Bub1 fluorescence, we create a projection of the
756 maximum values from all GFP sections, then divide the median fluorescence of the
757 brightest 5 pixels within each cell by the median fluorescence of the cell as a whole.
758 This ratio reliably measures protein aggregation at an organelle and has been
759 extensively used for quantification (Cai et al., 2008, Hao and O'Shea, 2011, Lin et al.,
760 2015). In the absence of nocodazole, cells with any outlier values for the ratio, defined
761 as values greater than 3 scaled median absolute deviations away from the median,
762 are removed. Cells present for fewer than 80% of recorded time points are also
763 removed. The ratios were normalized for each strain by dividing the mean value for
764 wild-type cells in the absence of nocodazole, measured in the same experiment. To
765 calculate the kinetochore retention times, a threshold of 1.36 (Figure 2F and G) and
766 1.11 (Supplementary Fig 4A and B) was applied to the ratio values at each time point
767 to determine the presence or absence of Bub1 at the kinetochore (Figure 2G and
768 Supplementary Fig 4B). Small gaps in localization (due to kinetochore signal dropping
769 briefly out of focus) were removed by applying a 1-dimensional morphological closing
770 to the thresholded image, with a 3-pixel (3 timepoint or 6 minutes) structuring element.
771 For the temporal heat maps (Figure 2F and Supplementary Fig 4A), the data for 30
772 cells present for the whole experiment are selected for inclusion from each strain
773 pseudo-randomly using the Matlab rand function. There were a small number of outlier
774 values within the heat maps, resulting from a fault in the LED control equipment. These
775 were removed by replacing any values in the 5th percentile of a cell trace with the
776 median value for all time points. The raw data and code used in data processing and
777 plotting are available on request.

778 **Flow cytometry**

779 5 mL of *C. neoformans* culture was grown overnight, and 2 $O.D_{600}$ cells were taken
780 and washed with sterile dH2O and fixed in 1 mL of 70% ethanol overnight at 4°C.
781 Fixed cells were centrifuged at 4000 rpm and washed with 1 mL NS buffer(10 mM
782 Tris-HCl pH 7.5, 250 mM sucrose, 1 mM EDTA (pH 8.0), 1 mM $MgCl_2$, 0.1 mM $CaCl_2$,
783 and 7 mM β-mercaptoethanol) and resuspended in 200 µL of NS buffer added with 2
784 µg of RNase and incubated at 37°C for 3-4 h. Propidium Iodide (final concentration 12
785 µg/mL) was added to this mixture and incubated for 30 min at room temperature in the
786 dark. 50 µL of the sample was suspended in 2 mL of 1x PBS (Phosphate buffered
787 saline) solution, vortexed, and sonicated for 10 s at 30% Amp. 30,000 cells were
788 analyzed by flow cytometry using FL2-A channel on (FACSAria III; BD Biosciences)
789 at a rate of 500–2,000 events/s.

790 **Western Blotting**

791 For immunoblotting, whole cell lysates were prepared by harvesting 10 $O.D_{600}$ cells
792 cultured using YPD. The cells were washed twice with sterile water and resuspended
793 in 15% TCA (Trichloroacetic acid), and samples were frozen in a -20°C freezer. The
794 cell suspension was thawed on ice and lysed using a mini-bead beater (Biospec
795 product) with 1 min ON and 5 min OFF for three cycles at 3000 RPM. The cell lysate
796 was centrifuged at 13000 RPM at 4°C for 10 min, and the supernatant was discarded.
797 The pellet was resuspended in 2x sample buffer (0.1 M Tris HCl pH 6.8, 20% glycerol,
798 4% SDS, 715 mM β-mercaptoethanol and 0.2% bromophenol blue) and incubated for
799 5 min in a boiling water bath. The samples were cleared by spinning at 13000 RPM
800 for 3 min, and the supernatant was loaded immediately onto an SDS-PAGE gel and
801 separated. The proteins were transferred to a PVDF membrane (Bio-Rad) using the
802 wet transfer method with a transfer time of two and a half hours at 90 V. The transfer
803 efficiency was estimated by staining the blot with Ponceau S solution. The membrane
804 was blocked using 3% skimmed milk and 2% BSA dissolved 1x PBST (0.1% Tween-
805 20) solution at room temperature for 60 minutes. Post blocking, the blot was incubated
806 in 2% skimmed milk and 1% BSA dissolved in 1x PBST solution containing anti-GFP
807 at 1:3000 dilution overnight at 4°C. The membrane was washed thrice for 10 min with
808 1x PBS solution containing 0.1% tween-20. The blot was incubated with an anti-mouse
809 secondary antibody (1:10000 dilution in 2% skimmed milk and 1% BSA dissolved in

810 1x PBST solution) for 1 hour at room temperature. The membrane was washed thrice
811 for 10 min with 1x PBS + 0.1% tween-20, and the blot was rinsed in 1x PBS and was
812 developed using Bio-Rad clarity ECL solution and imaged using Bio-Rad Chemidoc
813 imaging system.

814 **Chromatin Immunoprecipitation (ChIP)**

815 The ChIP protocol was adapted from (de Jonge et al., 2020, Mitra et al., 2014). ChIP
816 was performed in metaphase-arrested cells by depleting Scc1. Overnight cultures of
817 CNSD185 strain grown in 2% YPG (permissive media) were washed twice with 2%
818 YPD and inoculated at 0.2 $O.D_{600}$/mL in 150 mL of 2% YPD (Non-permissive) media.
819 The cells were grown for 6 h at 30°C, 180 RPM. Post 6 h incubation, the extent of
820 metaphase arrest was assessed using microscopy, and the culture was fixed by
821 adding freshly prepared methanol-free formaldehyde at 3% final concentration and
822 incubated at 25°C, 100 RPM for 35 minutes. The fixed cells were quenched with 1.5
823 M Tris HCl pH 8.0 for 5 mins at 25°C, 100 RPM. The cells were pelleted and washed
824 with ice-cold water flash frozen using liquid Nitrogen, and stored at -80°C. The cells
825 were lysed in a buffer containing 50 mM HEPES pH 7.4, 1% Triton-X, 140 mM NaCl,
826 0.1% Na-deoxycholate, 1 mM EDTA, 1x Protease Inhibitor Cocktail (Sigma) with 10
827 cycles of bead beating using a mini-beadbeater (BioSpec product) at 3500 RPM for 2
828 mins ON and 5 mins OFF on ice.

829 The lysate was transferred to a chilled 15 mL falcon on ice, and the cross-linked
830 chromatin was fragmented using an ultrasonicator (Diagenode Bioruptor Pico) at high
831 frequency, 30 s ON, 30 s OFF mode for 50 cycles to achieve the desired 250-500 size
832 range. The sample was transferred to a chilled 2 mL tube, and centrifuged at 10000
833 RPM for 10 min at 4°C. The debris-free supernatant was carefully transferred to a
834 fresh 2 mL tube and incubated with 20 µL of control trap beads (Chromo Tek) at 11
835 RPM for 3 h at 4°C. After incubation, bead-free supernatant was recovered by
836 centrifugation at 500 RCF for 2 min, and GFP-trap and block beads were added to the
837 respective tubes. The tubes were incubated at 11 RPM rotation for 12 h at 4°C. After
838 incubation, the beads were recovered by centrifugation at 1000 RCF for 1 min at RT,
839 and extensive washes were performed at RT with intermittent agitation at 11 RPM for
840 5 min. First, the beads were washed with 1 mL lysis buffer (50 mM HEPES pH 7.5,
841 140 mM NaCl, 1% Triton-X 100, 0.1% sodium deoxycholate, 2 mM PMSF), recovered

842 by centrifugation at 1000 RCF for 1 min at RT and then washed 2 times each with the
843 following buffers, with recovery at 1000 RCF for 1 min following each wash: (i) 20 mM
844 Tris HCl pH 8.0, 200 mM NaCl, 2 mM EDTA, 1% Triton-X-100, 0.1% SDS. (ii) 20 mM
845 Tris HCl pH 8.0, 500 mM NaCl, 2 mM EDTA, 1% Triton-X-100, 0.1% SDS. (iii) 20 mM
846 Tris HCl pH 8.0, 250 mM LiCl, 2 mM EDTA, 1% NP-40, 1% sodium-deoxycholate, pH
847 8.0. (iv) TE: 10 mM Tris HCl pH 8.0, 1 mM EDTA. The IP complex was recovered by
848 incubating the beads with 250 µL of elution buffer (10 mM Tris HCl pH 8.0, 1 mM
849 EDTA, 1% SDS, 200 mM NaCl) at 65°C for 15 min with intermittent flicking. The
850 process was repeated with another 250 µL buffer and pooled to obtain a 500 µL IP
851 sample. The input volume was adjusted to 500 µL with an elution buffer. For de-
852 crosslinking, 20 µL of 5 N NaCl was added to each sample and incubated overnight at
853 65°C. Next day, 20 µL 1M Tris-HCl pH 6.8, and 10 µL 0.5 M EDTA pH 8.0 were added
854 to each tube and treated with Proteinase K (2 µL/sample) at 42°C for 1 h followed by
855 RNase treatment (5 µL of 10 mg/mL RNase A/sample) at 37°C for 1 h. The DNA was
856 extracted with an equal volume of Tris pH 8.0-saturated phenol:chloroform:isoamyl
857 alcohol (25:24:1) and precipitated (with 1 mL of 100% ethanol with 100 µL 3 M sodium
858 acetate pH 5.3) overnight at -80°C. The DNA was pelleted by centrifugation at 14000
859 RPM for 30 min at 4°C, washed with chilled 70% ethanol, air-dried, and finally
860 resuspended in 20 µL TE pH 8.0. The ChIP-qPCR reactions were carried out in a total
861 10 µL volume using CEN and Non-CEN primers listed in Table S3.

862 **Statistics and microscope image analysis**

863 P-values were assessed by unpaired, two-tailed t-test or two-way ANOVA with Tukey's
864 multiple comparison test using GraphPad Prism 8.00 (GraphPad software). Error bars
865 represent the standard deviation (SD) or standard error of the mean (SEM) as
866 mentioned for each experiment. N for each experiment is mentioned in the figure
867 legends. Fiji software (Schindelin et al., 2012) was used to process and analyze
868 microscope images. Fluorescence intensity values of signals were quantified by
869 drawing a circular region of interest (ROI) of defined pixel size on the sum intensity Z-
870 projected images (Figure 2E, 3C and G) or on single Z-plane images (Figure 4C and
871 E). The intensity values were calculated by subtracting the product of mean
872 background fluorescence intensity and area of the ROI from integrated density, and
873 the resultant values were plotted using GraphPad Prism.

Acknowledgments

We thank members of the Sanyal laboratory for their support, discussion, and suggestions on the work. We thank A. A. Jeyaprakash, Institute of Cell Biology, School of Biological Sciences, University of Edinburgh, UK, for the discussion and suggestions on the work. We thank I. Leontiou and T. Davies (University of Edinburgh) for *bub1-kd* strain construction. We thank the in-house flow cytometry facility at JNCASR and N. Nala for assistance with flow cytometric analysis. We thank V. Yadav, Duke University, USA, for the reagents provided for Tub4-mCherry strain construction. S.D.P. is a Research Associate supported by SERB funding by the Government of India. KB is a senior research fellow (SRF) supported by CSIR, Government of India. KD is senior research fellow (SRF) supported by JNCASR. KH was supported by the Leverhulme Trust (RPG-2018-379); IC was supported by the Wellcome Trust-University of Edinburgh Institutional Strategic Support Fund, and we thank P. Swain (University of Edinburgh) for leading on this ISSF funding. KS is a JC Bose National Fellow (JCB/2020/000021) of the Science and Engineering Research Board (SERB), Department of Science and Technology, Government of India. Kaustuv Sanyal acknowledges financial support from the Department of Biotechnology, Government of India (IC-12025(22)/3/2023-ICD-DBT), SERB (CRG/2023/001077), and intramural funding from JNCASR.

Conflict of interest

The authors declare that they have no conflict of interest.

Declaration of interests

The authors declare no competing interests.

Figure legends

Figure 1. Shugoshin is required for a robust spindle assembly checkpoint arrest. **(A)** Schematic of the predicted motifs present in Sgo1 of *C. neoformans*. **(B)** A ten-fold serial dilution spotting assay to score for the sensitivity of strains CNVY108 (*SGO1 GFP-H4*), CNSD110 (*GFP-H4 sgo1Δ*), SHR741 (*GFP-H4 mad2Δ*), CNSD148 (*GFP-H4 sgo1Δ mad2Δ*) on plates containing the indicated concentrations of thiabendazole (TBZ). No drug represents DMF (dimethyl formamide) only. The plates were incubated at 30°C for 24 h. **(C)** *Left,* schematic of the assay to score for cell cycle arrest

905 phenotypes when treated with nocodazole. Cells treated with nocodazole for 120 and
906 240 min were scored for cell cycle arrest phenotypes. *Right,* bar graphs representing
907 the proportion of large-budded cells in the indicated strains, N=3, n>100, cells counted
908 in each experiment. Two-way ANOVA with Tukey's multiple comparison test was used
909 to estimate the significance. ****p<0.0001, ***p<0.001, **p=0.0019/0.0072. Non-
910 significant p-values were omitted from the graph. **(D)** *Left*, an outline of the assay to
911 study the effect of nocodazole on the ploidy content of indicated strains using flow
912 cytometry. *Right*, histograms depicting ploidy changes associated with nocodazole
913 treatment.

914 **Figure 2. Shugoshin ensures Bub1 is retained at kinetochores to maintain the**
915 **spindle assembly checkpoint arrest. (A)** Schematic of the SAC pathway and the
916 evolutionarily conserved role of Sgo1 and Aurora B^{Ipl1} in detecting erroneous
917 kinetochore-MT attachments. **(B)** An experimental workflow followed to determine the
918 GFP-Bub1 localization dynamics under nocodazole-treated conditions. **(C)** Sub-
919 cellular localization of GFP-Bub1 localization in IL102 (*SGO1*), IL143 (*bub1-kd*) and
920 CNSD176 (*sgo1Δ*). For representation, cells treated with nocodazole for 120 and 280
921 min were shown. Scale bar, 5 µm. **(D)** Quantification of the proportion of large-budded
922 cells with GFP-Bub1 signal in indicated strains treated with nocodazole. N=3, n>100
923 cells were analyzed, and the shaded regions above and below the line graphs
924 represent error bands corresponding to SD. **(E)** Quantification of GFP-Bub1
925 fluorescence intensity values at 120 min post-nocodazole treatment. N=3, n>100 cells
926 analyzed for each experiment. White circles represent the average intensity values of
927 replicates. A mean of the average intensity values of replicates is represented as a
928 black bar, and error bars represent SD. An unpaired t-test was used to test the
929 significance, ** p=0.0092, ns =0.1131 **(F)** Microfluidics assays to determine the
930 retention time of GFP-Bub1 at kinetochores in response to nocodazole treatment.
931 Temporal heat maps of 30 randomly selected cells are shown. The heat map
932 represents the changes in kinetochore localization signal of GFP-Bub1 over time.
933 Each bright track on the *y*-axis of the heat map represents GFP-Bub1 signals from an
934 individual cell (median of the brightest 5 pixels in each cell divided by the overall cell
935 median brightness). The length of each bright track along the *x*-axis represents the
936 time (min). The time of addition of nocodazole (2.5 µg/mL) is considered as 0 h.
937 Images are taken every 2 min for 15 h. Assays were performed using strains IL102

938 (*GFP-BUB1*), IL143 (*GFP-bub1-kd*), CNSD176 (*GFP-BUB1 sgo1Δ*), and IL089 (*GFP-*
939 *BUB1 mad1Δ*) strains. **(G)** Bar graphs representing the quantitative analysis of the
940 GFP-Bub1 retention time at kinetochores obtained from microfluidics assays in the
941 above-indicated strains. n=30, error bars represent SEM.

942 **Figure 3. Shugoshin-dependent Aurora B^{Ipl1} pool at kinetochores ensures**
943 **maintenance of Bub1 to prolong the checkpoint arrest. (A)** Sub-cellular
944 localization of Aurora B^{Ipl1}-3xGFP localization in CNSD190 (*AURORA B^{Ipl1}-3xGFP*
945 *mCherry-CENP-A SGO1*) and CNSD196 (*AURORA B^{Ipl1}-3xGFP mCherry-CENP-A*
946 *sgo1Δ*) strains treated with nocodazole. For representation, cells treated with
947 nocodazole for 120 and 280 min were shown. Scale bar, 5μm. **(B)** Quantification of
948 the proportion of large-budded cells with Aurora B^{Ipl1}-3xGFP signals in the indicated
949 strains. N=3, n>100 cells were analyzed, and the shaded regions above and below
950 the line graph represent error bands corresponding to SD. **(C)** Quantification of Aurora
951 B^{Ipl1}-3xGFP fluorescence intensity values at 120 min post-nocodazole treatment. N=3,
952 n>58 cells for each experiment. White circles represent the average intensity values
953 of replicates. The mean of the average intensity values of replicates is represented as
954 a black bar. Error bars represent SD. An unpaired t-test was used to test the
955 significance, ** p= 0.0013. **(D)** Schematic to assess the response of Aurora B^{Ipl1}
956 (over)expression or depletion to nocodazole treatment. **(E)** Sub-cellular localization of
957 GFP-Bub1 localization in CNSD205 (*GAL7-3xFLAG-AURORA B^{IPL1} GFP-BUB1*)
958 Aurora B^{Ipl1} (over)expressed and repressed conditions treated with nocodazole. Cells
959 treated with nocodazole for 120 and 240 min are shown for representation. Scale bar,
960 5 μm. **(F)** Bar graphs representing the proportion of large-budded cells with or without
961 of GFP-Bub1 signals at 120 and 240 min of nocodazole treatment. N=3, n>100 cells
962 analyzed for each experiment. Error bars represent SD. **(G)** Quantification of GFP-
963 Bub1 fluorescence intensity values in Aurora B^{Ipl1} (over)expressed and repressed
964 conditions at 120 min of nocodazole treatment. White circles represent the average
965 intensity values of replicates. The mean of the average intensity values of the
966 replicates is represented as a black bar. Error bars represent SD. N=3, n> 79 cells
967 analyzed for each experiment. An unpaired t-test was used to test the significance,
968 *p=0.0439.

969 **Figure 4. Sgo1-mediated Aurora B^{Ipl1} recruitment prevents excess PP1**
970 **phosphatase at the kinetochore. (A)** The effect of *sgo1Δ* on maintaining a balance

971 between Aurora B^{Ipl1} and PP1 levels at kinetochore in *C. neoformans*. **(B)** Sub-cellular
972 localization of CNKB003 (*GFP-PP1 mCherry-CENP-A SGO1*) and CNSD180 (*GFP-*
973 *PP1 mCherry-CENP-A sgo1Δ*) cells treated with nocodzole (1 µg/mL) for 120 min.
974 Yellow ovals highlight PP1-GFP signals. **(C)** Quantification of GFP-PP1 fluorescence
975 signal intensity values in the indicated strains treated with nocodazole. N=3, n>100
976 cells were analyzed for each experiment. White circles represent the average GFP-
977 PP1 signal intensities calculated for each experimental repeat. An unpaired t-test was
978 used to determine statistical significance. **p= 0.0044. The mean of the average
979 intensity values of replicates is represented as a black bar. Error bars represent SD.
980 **(D)** Microscopic images of CNKB023 (*GFP-PP1 mCherry-CENP-A GAL7-3xFLAG*
981 *AURORA B^{IPL1}*) Aurora B^{Ipl1} (over)expressed and repressed conditions treated with
982 nocodazole (1 µg/mL) for 120 min. **(E)** Quantification of fluorescence intensity values
983 of GFP-PP1 signals in conditions mentioned above. N=4, n=100 cells for each
984 experiment. White circles represent the average intensity values of replicates. Error
985 bars represent SD. The mean of the average intensity values plotted is represented
986 as a black bar. Paired t-test was used to determine statistical significance. **p= 0.0069.

987 **Figure 5. Kinetochore proximal association of Sgo1 in MT-depolymerizing**
988 **conditions. (A-D)** *Left,* microscopic images of GFP-Sgo1 localized with a kinetochore
989 marker, CENP-A, and an SPB marker, Tub4, at different stages of the mitotic cell
990 cycle, in nocodazole treated and Cdc20 depleted conditions. Scale bar, 5 µm. **(A)**
991 CNSD125 (*GFP-SGO1 mCherry-CENP-A*). **(B)** CNSD130 (*GFP-SGO1 TUB4-*
992 *mCherry*). **(C)** Nocodazole (1 µg/mL) treated condition. *Top panel*, CNSD125. *Bottom*
993 *panel*, CNSD130. **(D)** Cdc20 depletion condition, CNSD167 (*GFP-SGO1 mCherry-*
994 *CENP-A GAL7-3xFLAG-CDC20*). *Right*, line scan profiles of both GFP (Sgo1) and
995 mCherry (CENP-A, Tub4) fluorescence signals. Distance plotted on the *x*-axis
996 represents the length of the line drawn on the image to measure fluorescence
997 intensity. Gray values on the *y*-axis represent the fluorescence signal intensities.

998 **Figure 6. The kinase activity of Bub1 is dispensable for shugoshin-mediated**
999 **maintenance of the spindle assembly checkpoint. (A)** Schematic of the conserved
1000 pathway of shugoshin recruitment to kinetochores. **(B)** A ten-fold serial dilution
1001 spotting assay to score for the sensitivity of the CNSD110 (*sgo1Δ*), IL143 (*GFP-bub1-*
1002 *kd*), CNSD173 (*sgo1Δ GFP-bub1-kd*) double mutants and SHR866 (*mad2Δ*) to
1003 thiabendazole. **(C)** A ten-fold serial dilution spotting assay to score for the sensitivity

1004 of the CNSD125 (*GFP-SGO1 mCherry-CENP-A*), CNSD215 (*GFP-SGO1 mCherry-*
1005 *CENP-A bub1-kd-3XFLAG*), CNSD219 (*GFP-SGO1 mCherry-CENP-A h2a-T121A*),
1006 CNSD218 (*sgo1Δ GFP-sgo1-K382A-SH1 mCherry-CENP-A*), CNSD207 (*sgo1Δ*
1007 *GFP-SGO1-SH1*) and CNSD110 (*sgo1Δ*). **(D)** Microscopic images of GFP-Sgo1
1008 localized with CENP-A at metaphase stage in wild-type and mutant backgrounds.
1009 Scale bar, 5 μm. **(E)** *Top,* Schematic showing the line scan analysis method adopted
1010 to score for the fluorescence intensity of GFP-Sgo1 along the spindle and SPBs.
1011 *Middle,* line scan profile of GFP-Sgo1 in the indicated strains synchronized using
1012 thiabendazole (10 μg/mL) treatment. *Bottom*, line scan profile of GFP-Sgo1 in the
1013 indicated strains synchronized using hypoxia. Distance on the *x*-axis represents the
1014 length of the line drawn on the image to measure fluorescence intensity. The *y*-axis
1015 represents the fluorescence signal intensity values. N=3, n>20 cells were analysed for
1016 each experiment. Each line graph represents mean fluorescence intensity values
1017 calculated from three experimental repeats and error bars represent SD. **(F)** *Top,*
1018 Schematic of the assay used to arrest cells at metaphase by depleting Scc1. *Below*,
1019 microscopic images of GFP-Sgo1 localized with CENP-A metaphase in Scc1 depleted
1020 conditions. **(G)** Fold enrichment of Sgo1 at kinetochores in metaphase arrested cell
1021 obtained by cross-linking chromatin immunoprecipitation (ChIP) followed by
1022 quantitative polymerase chain reaction (qPCR). *CEN2* and *CEN5* represent
1023 centromeres 2 and 5, non-CEN region represents *LEU2* locus. N=3, and error bars
1024 represent SD.

1025 **Supplementary Figure legends**

1026 **Supplementary Figure 1. *C. neoformans* Sgo1, carrying a conserved coiled-coil**
1027 **domain and the SGO motif, is required to maintain SAC arrest in nocodazole-**
1028 **treated cells. (A)** The protein sequence of *C. neoformans* Sgo1. **(B)** Multiple
1029 sequence alignment (MSA) of the CnSgo1 N-terminal coiled-coil and the C-terminal
1030 SGO motif with vertebrate and invertebrate species (Cn- *C. neoformans*; Sc-
1031 *Saccharomyces cerevisiae*; Sp- *Schizosaccharomyces pombe*; Hs- *Homo sapiens*;
1032 Mm- *Mus musculus*; Xl- *Xenopus laevis*; Dm- *Drosophila melanogaster*). Multiple
1033 sequence alignment of Sgo1 homologs was performed using Clustal Omega (Sievers
1034 et al., 2011), and the alignment was formatted using Jalview 2 (Waterhouse et al.,
1035 2009). *Represent amino acid residues involved in PP2A binding. The dark blue circle
1036 represents the key residue (K382 in *C. neoformans*) required for Bub1-mediated

1037 kinetochore proximal centromere localization of shugoshin. The teal blue colored box
1038 represents the coiled-coil domain. The light blue colored box represents the conserved
1039 basic SGO motif. **(C)** Microscopic images of GFP-H4 in CNVY108 (*SGO1 MAD2*),
1040 CNSD117 (*sgo1Δ*), SHR866 (*mad2Δ*), CNSD148 (*sgo1Δ mad2Δ*) treated with
1041 nocodazole (1 µg/mL) for 120- and 240-min. Scale bar, 5 µm. **(D)** Bar graphs
1042 representing the proportion of unbudded, small-budded, large-budded, and tri-budded
1043 cells. N=3, n>100 cells counted in each experiment. **(E)** Bar graphs representing the
1044 proportion of large-budded cells of indicated phenotypes, N=3, n>100 cells counted in
1045 each experiment.

1046 **Supplementary Figure 2. *sgo1Δ bgi1Δ* double mutant cells exhibit enhanced**
1047 **sensitivity to MT depolymerizing drug.** A ten-fold serial dilution spotting assay to
1048 score for the sensitivity of the wild-type CNVY108 (*SGO1 BGI1 GFP-H4*), CNSD117
1049 (*sgo1Δ GFP-H4)*, SHR741 (*mad2Δ GFP-H4*), SHR830 (*bgi1Δ GFP-H4*), CNSD148
1050 (*sgo1Δ mad2Δ GFP-H4*) and CNSD163 (*sgo1Δ bgi1Δ GFP-H4*) to thiabendazole. No
1051 drug represents DMF (Dimethyl formamide) only. The plates were incubated at 30°C
1052 for 24 h.

1053 **Supplementary Figure 3. The proportion of large-budded cells scored for the**
1054 **presence or absence of GFP-Bub1 signal post nocodazole treatment.** Bar graphs
1055 representing the proportion of large-budded cells obtained post nocodazole treatment
1056 in the indicated strains, N=3, n>100, cells counted in each experiment. Errors bars
1057 represent SD.

1058 **Supplementary Figure 4. *bub1-kd sgo1Δ* double mutant cells behave similar to**
1059 **single *sgo1Δ* mutant cells. (A)** Microfluidics assay to determine the retention time of
1060 GFP-Bub1 at kinetochores in response to nocodazole treatment. Temporal heat maps
1061 of 30 randomly selected cells are shown. The heat map represents the changes in the
1062 kinetochore localization signal of GFP-Bub1 over time. Each bright track on the *y*-axis
1063 of the heat map represents GFP-Bub1 signals from an individual cell (median of the
1064 brightest 5 pixels in each cell divided by the overall cell median brightness). The length
1065 of each bright track along the *x*-axis represents the time (min). The time of addition of
1066 nocodazole (2.5 µg/mL) is considered as 0 hr. Images are taken every 2 min for 10 h.
1067 Assay was performed using IL102 (*GFP-BUB1*), IL143 (*GFP-bub1-kd*), CNSD176
1068 (*GFP-BUB1 sgo1Δ*), and CNSD173 (*GFP-bub1-kd sgo1Δ*) strains. **(B)** Bar graphs

1069 representing the quantitative analysis of GFP-Bub1 retention time at kinetochores
1070 obtained from microfluidics assays in the above-indicated strains. n=24, error bars
1071 represent SEM.

1072 **Supplementary Figure 5. Aurora B^{Ipl1} localizes to the kinetochore (CENP-A)**
1073 **during G2 and mitosis and exhibits spindle-like localization. (A)** Microscopic
1074 images of Aurora B^{Ipl1}-3xGFP localized with a kinetochore protein mCherry-CENP-A
1075 at G2, metaphase, and anaphase stages of the cell cycle. **(B)** Colocalization of Aurora
1076 B^{Ipl1}-3xGFP with mCherry-CENP-A when treated with nocodazole (1 µg/mL) for 120
1077 min. Scale bar, 5 µm.

1078 **Supplementary Figure 6. The proportion of large-budded cells scored for the**
1079 **presence or absence of Aurora B^{Ipl1}-3xGFP signal post nocodazole treatment.**
1080 Bar graphs representing the proportion of large-budded cells obtained post
1081 nocodazole treatment in the indicated strains, N=3, n>100, cells counted in each
1082 experiment. Errors bars represent SD.

1083 **Supplementary Figure 7. Aurora B^{Ipl1} mutants fail to arrest at metaphase in**
1084 **response to nocodazole treatment. (A)** Microscopic images of CNNV104 (*GFP-H4*
1085 *GAL7-AURORA B^{IPL1}*) grown in permissive and non-permissive media in the presence
1086 and absence of nocodazole. Scale bar, 5 µm. Representative images of cells treated
1087 with nocodazole and depleted of Aurora B^{Ipl1} for 240 and 480 min were shown. **(B)**
1088 *Left*, bar graphs representing the proportion of unbudded, small-budded, large-
1089 budded, and tri-budded cells. *Right*, bar graphs representing the proportion of large-
1090 budded cells of indicated phenotype, N=2, n>100 cells counted for each experiment.

1091 **Supplementary Figure 8. Sequence conservation of *C. neoformans* PP1.** Multiple
1092 sequence alignment of PP1 homolog of *C. neoformans* (CNAG_03706) with vertebrate
1093 and invertebrate species (Cn- *C. neoformans*; Sc- *S. cerevisiae*; Sp- *S. pombe*; Ca-
1094 *Candida albicans*; Hs- *H. sapiens*; Mm- *M. musculus*; Dm- *D. melanogaster*) was
1095 performed using Clustal Omega (Sievers et al., 2011) and the alignment was formatted
1096 using Jalview 2 (Waterhouse et al., 2009). Highly conserved regions are shaded in
1097 dark blue.

1098 **Supplementary Figure 9. Shugoshin responds to tensionless kinetochore-MT**
1099 **attachments. (A)** Pairwise sequence alignment of Scc1 homologs of *C. neoformans*
1100 (CNAG_01023) and *S. cerevisiae* by Clustal Omega (Sievers et al., 2011), and

1101 formatted using Jalview 2 (Waterhouse et al., 2009). Highly conserved regions are
1102 shaded in dark blue. The two domains corresponding to N- and C-terminal Scc1
1103 domains (E-values of 2.0e-31 and 2.2e-15, respectively) of CnScc1 are highlighted in
1104 violet and green boxes. **(B)** Schematic of the domains present in *C. neoformans* Scc1
1105 protein. **(C)** Plate photographs of strains expressing Scc1 under the regulatable *GAL7*
1106 promoter grown in media containing glucose (non-permissive) and galactose
1107 (permissive). **(D)** Schematic to check the response of Scc1 repression in *SGO1* and
1108 *sgo1Δ* backgrounds. **(E)** Microscopic images of GFP-H4 tagged CNSD181 (*GAL7-*
1109 *3xFLAG-SCC1*) and CNSD182 (*sgo1Δ GAL7-3xFLAG-SCC1*) strains depleted of
1110 Scc1. Representative images of cells depleted of Scc1 for 4 and 6 h were shown.
1111 Scale bar, 5 µm. **(F)** Bar graphs representing the percentage of unbudded, small-
1112 budded, large-budded, and tri-budded cells scored. N=2, n>100 cells for each
1113 experiment, error bars represent SD.

1114 **Supplementary Figure 10. Conservation of histone H2A sequence in *C.***
1115 ***neoformans* and expression levels of GFP-Sgo1 in various mutant strains. (A)**
1116 Multiple sequence alignment of H2A homologs obtained from *C. neoformans* (Cn)*, S.*
1117 *cerevisiae* (Sc), *S. pombe* (Sp) and *H. sapiens* (Hs). The alignment was performed
1118 using Clustal Omega (Sievers et al., 2011) and formatted using Jalview 2 (Waterhouse
1119 et al., 2009). The dark blue shaded regions represent highly conserved amino acid
1120 residues. Arrow indicates the conserved T121/S120 residue phosphorylated by Bub1.
1121 **(B)** Western blot showing the expression levels of GFP-Sgo1 at metaphase in the
1122 indicated strains. * Indicates non-specific band used as a loading control. Arrows
1123 indicate two bands of GFP-Sgo1. *sgo1Δ* lane represents no tag control.

1124 **Supplementary Figure 11. Schematic highlighting the sub-cellular localization**
1125 **of shugoshin reported in various species.** *Left*, schematic highlighting the spatial
1126 positioning of SPB/centrosome and centromeres in yeasts and metazoans. *Right*,
1127 localization of shugoshin with respect to the kinetochore, MTOCs (centrosomes or
1128 SPBs), spindle MTs, and telomeres. Filled and open squares represent the presence
1129 or absence of shugoshin at the indicated sub-cellular locations. The data was compiled
1130 from reviews (Marston, 2015, Gutierrez-Caballero et al., 2012). [1,2] (Mohr et al., 2015,
1131 Wang et al., 2008), [3*] (Salic et al., 2004), this study has shown that the purified N-
1132 terminal region of shugoshin is capable of binding to MTs *in* vitro. [4] (Sane et al., 2021)
1133 and [5] (Tashiro et al., 2016).

1134 **Table S1: List of strains**

Strain	Genotype	Source
H99	*MATα* (wild-type)	(Perfect et al., 1993)
CNVY101	*MATa::mCherry-CENP-A-NEO (pLKB74)*	(Kozubowski et al., 2013)
CNVY108	*MATα::GFP-H4-NAT (pVY3)*	(Kozubowski et al., 2013)
SHR741	*MATα::GFP-H4-NAT (pVY3) MAD2::mad2-NEO*	(Sridhar et al., 2021)
SHR830	*MATα::GFP-H4-NAT (pVY3) BGI1::bgi1Δ-HygB*	(Sridhar et al., 2021)
IL143	*MATα::BUB1::bub1Δ-NAT HISp-GFP-bub1-kd-HYGB (chromosome 3, safe haven p37)*	(Leontiou et al., 2022)
IL102	*MATα::BUB1::bub1Δ-NAT HISp-GFP-bub1-HygB (chromosome 3, safe haven p37)*	(Leontiou et al., 2022)
IL089	*MATα::MAD1::mad1Δ HISp:GFP-Bub1: HygB (chromosome 3, safe haven p37)*	(Leontiou et al., 2022)
CNNV113	*MATα:: AURK B^{IPL1}:: AURK B^{IPL1}p- AURK B^{IPL1}-3xGFP-NEO*	(Varshney et al., 2019)
CNNV104	*MATα:GFP-H4-NAT (pVY3), AURK B^{IPL1}::GAL7p- AURK B^{IPL1}- HygB*	(Varshney et al., 2019)
CNSD110	*MATα::SGO1::sgo1Δ-NEO*	This Study
CNSD117	*MATα::GFP-H4-NAT (pVY3) SGO1::sgo1Δ-NEO*	This Study
CNSD125	*MATa::mCherry-CENP-A-NEO (pLKB74) SGO1::SGO1pr-GFP-SGO1-NAT (pSD10)*	This study
CNSD127	*MATα::SGO1::SGO1p-GFP-SGO1-NAT (pSD10)*	This study
CNSD130	*MATα::SGO1::SGO1p-GFP-SGO1-NAT (pSD10) TUB4::TUB4-mCherry-NEO*	This study
CNSD148	*MATα::GFP-H4-NAT (pVY3) MAD2::mad2-NEO SGO1::sgo1Δ-NEO*	This study
CNSD163	*MATα::GFP-H4-NAT (pVY3) BGI1::bgi1Δ- HygB SGO1::sgo1Δ-NEO*	This study
CNSD167	*MATa::mCherry-CENP-A-NEO (pLKB74) SGO1::SGO1pr-GFP-SGO1-NAT (pSD10) CDC20p::GAL7p-3xFLAG-CDC20-HYGB*	This study
CNSD173	*MATα::BUB1::bub1Δ-NAT HISp-GFP-bub1-kd-HygB (chromosome 3, safe haven p37) SGO1::sgo1Δ-NEO*	This study

CNSD176	*MATα::BUB1::bub1Δ-NAT HISp-GFP-bub1-HygB (chromosome 3, safe haven p37) SGO1::sgo1Δ-NEO*	This study
CNSD180	*MATa::mcherry-CENP-A-NEO PP1:: PP1p-GFP-PP1-NAT* (pKB004) *SGO1::sgo1Δ-HYGB*	This study
CNSD181	*MATα::GFP-H4-NAT (pVY3) SCC1p::GAL7p-3xFLAG-SCC1- HygB*	This study
CNSD182	*MATα::GFP-H4-NAT (pVY3) SCC1p::GAL7p-3xFLAG-SCC1- HygB SGO1::sgo1Δ-NEO*	This study
CNSD183	*MATa::mCherry-CENP-A-NEO (pLKB74) SGO1::SGO1pr-GFP-SGO1-NAT (pSD10) SCC1p::GAL7p-3xFLAG-SCC1- HygB*	This study
CNSD190	*MATα::AURK B^{IPL1}:: AURK B^{IPL1}p- AURK B^{IPL1}-3xGFP-NEO mCherry-CENP-A- HygB (pLKB71)*	This study
CNSD196	*MATα:: AURK B^{IPL1}:: AURK B^{IPL1}p- AURK B^{IPL1}-3xGFP-NEO mCherry-CENP-A-HygB (pLKB71) SGO1::sgo1Δ-NAT*	This study
CNSD205	*MATα::BUB1::bub1Δ-NAT HISp-GFP-bub1-HygB (chromosome 3, safe haven p37) AURK B^{IPL1}::GAL7-3xFLAG-AUR B^{IPL1}-NEO*	This study
CNSD207	*MATα::SGO1::sgo1Δ-NEO SGO1p-GFP-SGO1-HygB (pSD34) (SAFE HAVEN1, chrormosome1)*	This study
CNSD209	*MATα::SGO1::sgo1Δ-NEO SGO1p-GFP-sgo1-K382A- HygB (pSD35) (SAFE HAVEN1, chrormosome1)*	This study
CNSD215	*MATa::mCherry-CENP-A-NEO (pLKB74) SGO1::SGO1pr-GFP-SGO1-NAT (pSD10) Bub1-kd-3xFLAG-HygB* (*pSD39*)	This study
CNSD218	*MATα::SGO1::sgo1Δ-NEO SGO1p-GFP-sgo1-K382A- HygB (pSD35) (SAFE HAVEN1, chrormosome1)*	This study
CNSD219	*MATα::SGO1::sgo1Δ-NEO SGO1p-GFP-sgo1-K382A- HygB (pSD35) (SAFE HAVEN1, chrormosome1) mCherry-CENP-A-NAT* (random integration) (*pSD41*)	This study
CNKB003	*MATa::mcherry-CENP-A-NEO PP1:: PP1p-GFP-PP1-NAT* (pKB004)	This study
CNKB023	*MATa::mcherry-CENP-A-NEO PP1:: PP1p-GFP-PP1-NAT* (pKB004) *AURK B^{IPL1}::GAL7-3XFLAG-AURK B^{IPL1}-NEO*	This study

1135 **Table S2: List of plasmids**

Plasmid	Description	Source
pVY7	*H3p-GFP-NAT* from pCN19 cloned into pBSII using SacI-ApaI	(Yadav and Sanyal, 2018)
pSH7G	*HygB-GAL7-GFP* pBlueScriptII KS(-)	(Sridhar et al., 2021)
pLKB71	pXLI + *mCherry-CENP-A-HygB*	From Joseph Heitman, Duke University, US
pSD10	*H3p* of pVY7 replaced with *SGO1p* (SacI/NcoI) + *SGO1* homology region (BamHI)	This study
pSD29	*GAL7p of p*SH7G replaced with *SGO1p* (SpeI/BamHI)+*SGO1* 3'UTR (NheI/ApaI)+*SAFE HAVEN1* (ApaI)	This study
pSD34	*SGO1* allele (HpaI/NheI) cloned into pSD29	This study
pSD35	*sgo1-K382A* allele (HpaI/NheI) cloned into pSD29	This study
pSD39	*GAL7-GFP of pSH7G replaced with bub1-kd* homology region harbouring *K1011R* and *D1149N* (SpeI/KpnI)	This study
pSD41	pXLI + *mCherry-CENP-A-NAT*	This study
pKB004	*H3p* of pVY7 replaced with *PP1p* (SacI/NcoI) +*PP1* homology region (SpeI)	This study

1136 **Table S3: List of primers**

Primer number	Sequence 5'-3'	Purpose
SDP1	CCGATGAGCGTACACCACTTAC	*SGO1* deletion overlap primers
SDP2	CCAGCTCACATCCTCGCAGCTGCTACGAGATTGAGACGAATG	
SDP3	CATTCGTCTCAATCTCGTAGCAGCTGCGAGGATGTGAGCTGG	
SDP4	CTCCCAACTTCCCCGCTTTTGGTTTATCTGTATTAACACGGAAGAG	
SDP5	CTCTTCCGTGTTAATACAGATAAACCAAAAGCGGGGAAGTTGGGAG	
SDP6	ATCAGAACGCACGTCGCAC	
SDP7	CAGGCAGAGGATTGGGAAGTC	
SDP8	CCAGTTCCTCAAAGAGCTTGAC	*SGO1* deletion confirmation primer
SDP20	ACTGAGCTCACTATCTGCAAAATCGACTTG	*SGO1pr-GFP-SGO1* N-terminal tagging
SDP21	CATGCCATGGCCTGTATTTACGCCTGGAG	
SDP22	CGCGGATCCATGTCCCAGAGGCAAGGCAG	
SDP23	CGCGGATCCGTTTCATCTCGACCACAGGTC	
SDP24	GGCACAAGCTGGAGTACAAC	Universal forward primer for tagging confirmation
SDP25	CTTCAGGTTCAGCATTGTCTG	
SDP27	ACTGGGCCCACACGATGTTTTCCATCAG	*SAFE HAVEN1* cloning
SDP28	ACTGGGCCCGGTCTCACAATCATCAACATC	
SDP54	AACAGTGATGGCAGCGTC	*TUB4-mCherry* C-terminal tagging overlap
SDP55	CGCATCCAACGTCATCCAAG	
VYP360	CTTGTGAACAATGCTGATAGTGTGG	
VYP361	CTCGCCCTTGCTCACCATCTCCCCCCCAAAATCGATATAATCC	
VYP362	GGATTATATCGATTTTGGGGGGGAGATGGTGAGCAAGGGCGAG	
VYP363	CGAAGTGCGTACTTGAAAGAAGTCCAAGCTTGGTACCGAGCTC	
VYP364	GAGCTCGGTACCAAGCTTGGACTTCTTTCAAGTACGCACTTCG	
VYP365	TGATGATCTCCAAGCTCTTCAC	
SDP108	TTGTTGTTACCATCATCCTCTC	Universal confirmation Reverse primer for deletion cassettes
SDP110	AGATCGACAACATGCGACC	

SDP111	CTGCAGATATCCATCACACTGGGAAGGGACC GTTTTTGACTAAC	*GAL7-3xFLAG-Cdc20* tagging overlap
SDP112	GTTAGTCAAAAACGGTCCCTTCCCAGTGTGA TGGATATCTGCAG	
SDP113	ATGGTCTTTGTAGTCCATCATTCTCAGGAGA GAATTGAGTG	
SDP114	ATGGACTACAAAGACCATGACGGTGATTATA AAGATC ATGACATCGACTACAAGGATGACGATGACAA GCTTGGAGA ACATACATCTGGC	
SDP115	CCGTGCCAACTCATGACC	
SDP116	GGATGTCGGCAATGAATTCAG	*GAL7-3xFLAG-Cdc20* integration confirmation
SDP162	AGCCTCATCCGACTTCACAG	*GAL7-3xFLAG-SCC1* tagging overlap
SDP163	GCAGATATCCATCACACTGGCCAACACGTAC ACGTCAACC	
SDP164	GGTTGACGTGTACGTGTTGGCCAGTGTGATG GATATCTGC	
SDP165	CACCGTCATGGTCTTTGTAGTCCATTCTCAG GAGAGAATTG AGTGC	
SDP166	ATGGACTACAAAGACCATGACGGTGATTATA AAGATCATGA CATCGACTACAAGGATGACGATGACAAGATC TTGAACGAAC TGATCAAGTC	
SDP167	CCATCTCGACATCATAGTCGTC	
SDP168	CCTTACGACCACAACCAGC	*GAL7-3xFLAG-SCC1* integration confirmation
SDP191	TATGACCTAGAACTGACAGACTCG	*GAL7-3xFLAG-AURK B^{IPL1} tagging overlap*
SDP192	GCAGATATCCATCACACTGGGGAGGCCAAAT CTGGAGG	
SDP193	CCTCCAGATTTGGCCTCCCCAGTGTGATGGA TATCTGC	
SDP195	ATGGACTACAAAGACCATGACGGTGATTATA AAGATCATGACATCGACTACAAGGAT GACGATGACAAGTCCTCGCAGAATGTTTCTG G	

SDP196	CTCGTCAAATCTGCCTAATCTGG	
SDP197	GTCCTGTAGAAGTTGAATTGC	*GAL7-3xFLAG-AURK B*^{IPL1} integration confirmation
SDP170	TTCGTCGACAACGCTAGCTAATGGCGACGATAATGATG	*SGO1* 3'UTR cloning for complementation
SDP171	TATGGGCCCTGCACTTGCGATAGATATCG	
SDP172	ACTGTTAACATGTCCCAGAGGCAAGGC	*SGO1* gene amplification for sgo1 deletion complementation
SDP173	GTTGCTAGCTTACTGCAAGACTCCAACGGC	
SDP198	CCCATCAGGTTTCCGCATGGCTCTTTCGAAATTATCAGCTAACG	*sgo1-K382A* allele amplification for sgo1 deletion complementation
SDP199	CGTTAGCTGATAATTTCGAAAGAGCCATGCGGAAACCTGATGGG	
SDP201	CTGAAGGAACTGGAAGAGG	*sgo1-K382A* sequencing primer
SDP212	GTGACTAGTAGGCGCTCTTCTGTCGAG	
SDP213	TCAGGTACCCTACTTGTCATCGTCATCCTTGTAGTCGATGTCATGATCTTTATAATCACCGTCATGGTCTTTGTAGTCAAGCTTCCTTGAAGTCGTAG	*bub1-kd* homology cloning primers
SDP214	ATGTCTTCCGGTGGCAAAGGC	*h2a-T121A* overlap cassette primers
SDP215	GCCTTGGCCTTGCCCTTAGCCTATGATATACATCAGCTGCTGATC	
SDP216	GATCAGCAGCTGATGTATATCATAGGCTAAGGGCAAGGCCAAGGC	
SDP217	GATATCCATCACACTGGCGCATCTCCTACTCATCGGCCATCAG	
SDP218	CTGATGGCCGATGAGTAGGAGATGCGCCAGTGTGATGGATATC	
SDP219	GGTTCATCAACAATTGTAATTCTCGGTTTATCTGTATTAACAC	
SDP220	GTGTTAATACAGATAAACCGAGAATTACAATTGTTGATGAACC	
SDP221	GATCTCCTCTGTGTCGGACATG	
SDP222	CCATCCAACAAGTCTTTCC	*h2a-T121A* sequencing and confirmation primer
SDP223	CTCCACACAAGAGACTCC	

SDP224	CAGCTATGACCATGATTACG	*bub1-kd-3xFLAG* confirmation primers
KBP001	ACGGAGCTCGACGTCGTACAAATGCATAC	*GFP-PP1* N-terminal tagging
KBP002	GGCCCATGGTTTATACGAAGTACGTTATATGTG	*GFP-PP1* N-terminal tagging
KBP003	TATACTAGTATGGGAGAACAGCCTGAAATTG	
KBP005	ATCACTAGTCAATAAACAAGCTCACTTGGAAGG	
KBP006	GCCGCCGTATCCACCGTATTTC	
VYP51	TTGAATCCTGCAGATCACAC	*CEN5* qPCR primers
VYP52	CAGCACAGTCAGTTTCATG	
VYP67	CAGACCCTTCCTTCAGCCG	*CEN2* qPCR primers
VYP68	TGGCAAGGAGTCGTCAGCG	

1137 ## References

1138 AKTAR, K., DAVIES, T., LEONTIOU, I., CLARK, I., SPANOS, C., WALLACE, E., TUCK, L., JEYAPRAKASH, A. A.
1139 & HARDWICK, K. G. 2024. Conserved signalling functions for Mps1, Mad1 and Mad2 in the
1140 Cryptococcus neoformans spindle checkpoint. *PLoS Genet,* 20**,** e1011302.

1141 ARRAS, S. D., CHITTY, J. L., BLAKE, K. L., SCHULZ, B. L. & FRASER, J. A. 2015. A genomic safe haven for
1142 mutant complementation in Cryptococcus neoformans. *PLoS One,* 10**,** e0122916.

1143 AUDETT, M. R., JOHNSON, E. L., MCGORY, J. M., BARCELOS, D. M., SZALAI, E. O., PRZEWLOKA, M. R. &
1144 MARESCA, T. J. 2022. The microtubule- and PP1-binding activities of Drosophila melanogaster
1145 Spc105 control the kinetics of SAC satisfaction. *Mol Biol Cell,* 33**,** ar1.

1146 BIGGINS, S. & MURRAY, A. W. 2001. The budding yeast protein kinase Ipl1/Aurora allows the absence
1147 of tension to activate the spindle checkpoint. *Genes Dev,* 15**,** 3118-29.

1148 BOYARCHUK, Y., SALIC, A., DASSO, M. & ARNAOUTOV, A. 2007. Bub1 is essential for assembly of the
1149 functional inner centromere. *J Cell Biol,* 176**,** 919-28.

1150 CAI, L., DALAL, C. K. & ELOWITZ, M. B. 2008. Frequency-modulated nuclear localization bursts
1151 coordinate gene regulation. *Nature,* 455**,** 485-90.

1152 CHEESEMAN, I. M., CHAPPIE, J. S., WILSON-KUBALEK, E. M. & DESAI, A. 2006. The conserved KMN
1153 network constitutes the core microtubule-binding site of the kinetochore. *Cell,* 127**,** 983-97.

1154 CIFERRI, C., PASQUALATO, S., SCREPANTI, E., VARETTI, G., SANTAGUIDA, S., DOS REIS, G., MAIOLICA,
1155 A., POLKA, J., DE LUCA, J. G., DE WULF, P., SALEK, M., RAPPSILBER, J., MOORES, C. A., SALMON,
1156 E. D. & MUSACCHIO, A. 2008. Implications for kinetochore-microtubule attachment from the
1157 structure of an engineered Ndc80 complex. *Cell,* 133**,** 427-39.

1158 COHEN-FIX, O., PETERS, J. M., KIRSCHNER, M. W. & KOSHLAND, D. 1996. Anaphase initiation in
1159 Saccharomyces cerevisiae is controlled by the APC-dependent degradation of the anaphase
1160 inhibitor Pds1p. *Genes Dev,* 10**,** 3081-93.

1161 CRANE, M. M., CLARK, I. B., BAKKER, E., SMITH, S. & SWAIN, P. S. 2014. A microfluidic system for
1162 studying ageing and dynamic single-cell responses in budding yeast. *PLoS One,* 9**,** e100042.

1163 DAVIDSON, R. C., CRUZ, M. C., SIA, R. A., ALLEN, B., ALSPAUGH, J. A. & HEITMAN, J. 2000. Gene
1164 disruption by biolistic transformation in serotype D strains of Cryptococcus neoformans.
1165 *Fungal Genet Biol,* 29**,** 38-48.

1166 DE JONGE, W. J., BROK, M., KEMMEREN, P. & HOLSTEGE, F. C. P. 2020. An Optimized Chromatin
1167 Immunoprecipitation Protocol for Quantification of Protein-DNA Interactions. *STAR Protoc,* 1**,**
1168 100020.

1169 ESPEUT, J., CHEERAMBATHUR, D. K., KRENNING, L., OEGEMA, K. & DESAI, A. 2012. Microtubule binding
1170 by KNL-1 contributes to spindle checkpoint silencing at the kinetochore. *J Cell Biol,* 196**,** 469-
1171 82.

1172 FERNIUS, J. & HARDWICK, K. G. 2007. Bub1 kinase targets Sgo1 to ensure efficient chromosome
1173 biorientation in budding yeast mitosis. *PLoS Genet,* 3**,** e213.

1174 GRANADOS, A. A., CRANE, M. M., MONTANO-GUTIERREZ, L. F., TANAKA, R. J., VOLIOTIS, M. & SWAIN,
1175 P. S. 2017. Distributing tasks via multiple input pathways increases cellular survival in stress.
1176 *Elife,* 6.

1177 GRANADOS, A. A., PIETSCH, J. M. J., CEPEDA-HUMEREZ, S. A., FARQUHAR, I. L., TKACIK, G. & SWAIN, P.
1178 S. 2018. Distributed and dynamic intracellular organization of extracellular information. *Proc*
1179 *Natl Acad Sci U S A,* 115**,** 6088-6093.

1180 GUACCI, V., KOSHLAND, D. & STRUNNIKOV, A. 1997. A direct link between sister chromatid cohesion
1181 and chromosome condensation revealed through the analysis of MCD1 in S. cerevisiae. *Cell,*
1182 91**,** 47-57.

1183 GUTIERREZ-CABALLERO, C., CEBOLLERO, L. R. & PENDAS, A. M. 2012. Shugoshins: from protectors of
1184 cohesion to versatile adaptors at the centromere. *Trends Genet,* 28**,** 351-60.

1185 HAO, N. & O'SHEA, E. K. 2011. Signal-dependent dynamics of transcription factor translocation
1186 controls gene expression. *Nat Struct Mol Biol,* 19**,** 31-9.

1187 HARDWICK, K. G., JOHNSTON, R. C., SMITH, D. L. & MURRAY, A. W. 2000. MAD3 encodes a novel
1188 component of the spindle checkpoint which interacts with Bub3p, Cdc20p, and Mad2p. *J Cell*
1189 *Biol,* 148**,** 871-82.

1190 HAUF, S., COLE, R. W., LATERRA, S., ZIMMER, C., SCHNAPP, G., WALTER, R., HECKEL, A., VAN MEEL, J.,
1191 RIEDER, C. L. & PETERS, J. M. 2003. The small molecule Hesperadin reveals a role for Aurora B
1192 in correcting kinetochore-microtubule attachment and in maintaining the spindle assembly
1193 checkpoint. *J Cell Biol,* 161**,** 281-94.

1194 HEITMAN, J. 2011. Microbial Pathogens in the Fungal Kingdom. *Fungal Biol Rev,* 25**,** 48-60.

1195 HINDRIKSEN, S., LENS, S. M. A. & HADDERS, M. A. 2017. The Ins and Outs of Aurora B Inner Centromere
1196 Localization. *Front Cell Dev Biol,* 5**,** 112.

1197 HWANG, L. H., LAU, L. F., SMITH, D. L., MISTROT, C. A., HARDWICK, K. G., HWANG, E. S., AMON, A. &
1198 MURRAY, A. W. 1998. Budding yeast Cdc20: a target of the spindle checkpoint. *Science,* 279**,**
1199 1041-4.

1200 INDJEIAN, V. B., STERN, B. M. & MURRAY, A. W. 2005. The centromeric protein Sgo1 is required to
1201 sense lack of tension on mitotic chromosomes. *Science,* 307**,** 130-3.

1202 KALLIO, M. J., MCCLELAND, M. L., STUKENBERG, P. T. & GORBSKY, G. J. 2002. Inhibition of aurora B
1203 kinase blocks chromosome segregation, overrides the spindle checkpoint, and perturbs
1204 microtubule dynamics in mitosis. *Curr Biol,* 12**,** 900-5.

1205 KAWASHIMA, S. A., YAMAGISHI, Y., HONDA, T., ISHIGURO, K. & WATANABE, Y. 2010. Phosphorylation
1206 of H2A by Bub1 prevents chromosomal instability through localizing shugoshin. *Science,* 327**,**
1207 172-7.

1208 KIBURZ, B. M., REYNOLDS, D. B., MEGEE, P. C., MARSTON, A. L., LEE, B. H., LEE, T. I., LEVINE, S. S.,
1209 YOUNG, R. A. & AMON, A. 2005. The core centromere and Sgo1 establish a 50-kb cohesin-
1210 protected domain around centromeres during meiosis I. *Genes Dev,* 19**,** 3017-30.

1211 KING, R. W., DESHAIES, R. J., PETERS, J. M. & KIRSCHNER, M. W. 1996. How proteolysis drives the cell
1212 cycle. *Science,* 274**,** 1652-9.

1213 KITAJIMA, T. S., KAWASHIMA, S. A. & WATANABE, Y. 2004. The conserved kinetochore protein
1214 shugoshin protects centromeric cohesion during meiosis. *Nature,* 427**,** 510-7.

1215 KOZUBOWSKI, L., YADAV, V., CHATTERJEE, G., SRIDHAR, S., YAMAGUCHI, M., KAWAMOTO, S., BOSE,
1216 I., HEITMAN, J. & SANYAL, K. 2013. Ordered kinetochore assembly in the human-pathogenic
1217 basidiomycetous yeast Cryptococcus neoformans. *mBio,* 4**,** e00614-13.

1218 KRONSTAD, J. W., ATTARIAN, R., CADIEUX, B., CHOI, J., D'SOUZA, C. A., GRIFFITHS, E. J., GEDDES, J. M.,
1219 HU, G., JUNG, W. H., KRETSCHMER, M., SAIKIA, S. & WANG, J. 2011. Expanding fungal
1220 pathogenesis: Cryptococcus breaks out of the opportunistic box. *Nat Rev Microbiol,* 9**,** 193-
1221 203.

1222 LARA-GONZALEZ, P., PINES, J. & DESAI, A. 2021. Spindle assembly checkpoint activation and silencing
1223 at kinetochores. *Semin Cell Dev Biol,* 117**,** 86-98.

1224 LEONTIOU, I., DAVIES, T., CLARK, I., AKTAR, K., SURESH, A. P., ABAD, M. A., SPANOS, C., LEE, K.-T.,
1225 BAHN, Y.-S., JEYAPRAKASH, A. A. & HARDWICK, K. G. 2022. Bub1 kinase acts as a signalling hub
1226 for the entire Cryptococcus neoformans spindle assembly checkpoint pathway. *bioRxiv***,**
1227 2022.09.21.508923.

1228 LESAGE, B., QIAN, J. & BOLLEN, M. 2011. Spindle checkpoint silencing: PP1 tips the balance. *Curr Biol,*
1229 21**,** R898-903.

1230 LIN, Y., SOHN, C. H., DALAL, C. K., CAI, L. & ELOWITZ, M. B. 2015. Combinatorial gene regulation by
1231 modulation of relative pulse timing. *Nature,* 527**,** 54-8.

1232 LIU, D., VLEUGEL, M., BACKER, C. B., HORI, T., FUKAGAWA, T., CHEESEMAN, I. M. & LAMPSON, M. A.
1233 2010. Regulated targeting of protein phosphatase 1 to the outer kinetochore by KNL1 opposes
1234 Aurora B kinase. *J Cell Biol,* 188**,** 809-20.

1235 LIU, H., JIA, L. & YU, H. 2013. Phospho-H2A and cohesin specify distinct tension-regulated Sgo1 pools
1236 at kinetochores and inner centromeres. *Curr Biol,* 23**,** 1927-33.

1237 LUO, J., DENG, X., BUEHL, C., XU, X. & KUO, M. H. 2016. Identification of Tension Sensing Motif of
1238 Histone H3 in Saccharomyces cerevisiae and Its Regulation by Histone Modifying Enzymes.
1239 *Genetics,* 204**,** 1029-1043.

1240 LUO, J., XU, X., HALL, H., HYLAND, E. M., BOEKE, J. D., HAZBUN, T. & KUO, M. H. 2010. Histone h3 exerts
1241 a key function in mitotic checkpoint control. *Mol Cell Biol,* 30**,** 537-49.

1242 MARSTON, A. L. 2015. Shugoshins: tension-sensitive pericentromeric adaptors safeguarding
1243 chromosome segregation. *Mol Cell Biol,* 35**,** 634-48.

1244 MEADOWS, J. C., SHEPPERD, L. A., VANOOSTHUYSE, V., LANCASTER, T. C., SOCHAJ, A. M., BUTTRICK,
1245 G. J., HARDWICK, K. G. & MILLAR, J. B. 2011. Spindle checkpoint silencing requires association
1246 of PP1 to both Spc7 and kinesin-8 motors. *Dev Cell,* 20**,** 739-50.

1247 MICHAELIS, C., CIOSK, R. & NASMYTH, K. 1997. Cohesins: chromosomal proteins that prevent
1248 premature separation of sister chromatids. *Cell,* 91**,** 35-45.

1249 MISHRA, P. K., THAPA, K. S., CHEN, P., WANG, S., HAZBUN, T. R. & BASRAI, M. A. 2018. Budding yeast
1250 CENP-A(Cse4) interacts with the N-terminus of Sgo1 and regulates its association with
1251 centromeric chromatin. *Cell Cycle,* 17**,** 11-23.

1252 MITRA, S., GOMEZ-RAJA, J., LARRIBA, G., DUBEY, D. D. & SANYAL, K. 2014. Rad51-Rad52 mediated
1253 maintenance of centromeric chromatin in Candida albicans. *PLoS Genet,* 10**,** e1004344.

1254 MOHR, L., BUHEITEL, J., SCHOCKEL, L., KARALUS, D., MAYER, B. & STEMMANN, O. 2015. An
1255 Alternatively Spliced Bifunctional Localization Signal Reprograms Human Shugoshin 1 to
1256 Protect Centrosomal Instead of Centromeric Cohesin. *Cell Rep,* 12**,** 2156-68.

1257 MUSACCHIO, A. 2015. The Molecular Biology of Spindle Assembly Checkpoint Signaling Dynamics. *Curr*
1258 *Biol,* 25**,** R1002-18.

1259 MUSACCHIO, A. & DESAI, A. 2017. A Molecular View of Kinetochore Assembly and Function. *Biology*
1260 *(Basel),* 6.

1261 MUSACCHIO, A. & SALMON, E. D. 2007. The spindle-assembly checkpoint in space and time. *Nat Rev*
1262 *Mol Cell Biol,* 8**,** 379-93.

1263 NG, T. M., LENSTRA, T. L., DUGGAN, N., JIANG, S., CETO, S., HOLSTEGE, F. C., DAI, J., BOEKE, J. D. &
1264 BIGGINS, S. 2013. Kinetochore function and chromosome segregation rely on critical residues
1265 in histones H3 and H4 in budding yeast. *Genetics,* 195**,** 795-807.

1266 NIJENHUIS, W., VALLARDI, G., TEIXEIRA, A., KOPS, G. J. & SAURIN, A. T. 2014. Negative feedback at
1267 kinetochores underlies a responsive spindle checkpoint signal. *Nat Cell Biol,* 16**,** 1257-64.

1268 NOGUEIRA, C., KASHEVSKY, H., PINTO, B., CLARKE, A. & ORR-WEAVER, T. L. 2014. Regulation of
1269 centromere localization of the Drosophila Shugoshin MEI-S332 and sister-chromatid cohesion
1270 in meiosis. *G3 (Bethesda),* 4**,** 1849-58.

1271 OHKUSU, M., RACLAVSKY, V. & TAKEO, K. 2004. Induced synchrony in Cryptococcus neoformans after
1272 release from G2-arrest. *Antonie Van Leeuwenhoek,* 85**,** 37-44.

1273 ORNER, E. P., ZHANG, P., JO, M. C., BHATTACHARYA, S., QIN, L. & FRIES, B. C. 2019. High-Throughput
1274 Yeast Aging Analysis for Cryptococcus (HYAAC) microfluidic device streamlines aging studies
1275 in Cryptococcus neoformans. *Commun Biol,* 2**,** 256.

1276 PEPLOWSKA, K., WALLEK, A. U. & STORCHOVA, Z. 2014. Sgo1 regulates both condensin and
1277 Ipl1/Aurora B to promote chromosome biorientation. *PLoS Genet,* 10**,** e1004411.

1278 PERFECT, J. R., KETABCHI, N., COX, G. M., INGRAM, C. W. & BEISER, C. L. 1993. Karyotyping of
1279 Cryptococcus neoformans as an epidemiological tool. *J Clin Microbiol,* 31**,** 3305-9.

1280 PETERSEN, J. & HAGAN, I. M. 2003. S. pombe aurora kinase/survivin is required for chromosome
1281 condensation and the spindle checkpoint attachment response. *Curr Biol,* 13**,** 590-7.

1282 PIETSCH, J. M. J., MUNOZ, A. F., ADJAVON, D. A., FARQUHAR, I., CLARK, I. B. N. & SWAIN, P. S. 2023.
1283 Determining growth rates from bright-field images of budding cells through identifying
1284 overlaps. *Elife,* 12.

1285 PINSKY, B. A., KUNG, C., SHOKAT, K. M. & BIGGINS, S. 2006. The Ipl1-Aurora protein kinase activates
1286 the spindle checkpoint by creating unattached kinetochores. *Nat Cell Biol,* 8**,** 78-83.

1287 PINSKY, B. A., NELSON, C. R. & BIGGINS, S. 2009. Protein phosphatase 1 regulates exit from the spindle
1288 checkpoint in budding yeast. *Curr Biol,* 19**,** 1182-7.

1289 RESNICK, T. D., SATINOVER, D. L., MACISAAC, F., STUKENBERG, P. T., EARNSHAW, W. C., ORR-WEAVER,
1290 T. L. & CARMENA, M. 2006. INCENP and Aurora B promote meiotic sister chromatid cohesion
1291 through localization of the Shugoshin MEI-S332 in Drosophila. *Dev Cell,* 11**,** 57-68.

1292 ROSENBERG, J. S., CROSS, F. R. & FUNABIKI, H. 2011. KNL1/Spc105 recruits PP1 to silence the spindle
1293 assembly checkpoint. *Curr Biol,* 21**,** 942-7.

1294 ROY, B., HAN, S. J. Y., FONTAN, A. N., JEMA, S. & JOGLEKAR, A. P. 2022. Aurora B phosphorylates Bub1
1295 to promote spindle assembly checkpoint signaling. *Curr Biol,* 32**,** 237-247 e6.

1296 ROY, B., VERMA, V., SIM, J., FONTAN, A. & JOGLEKAR, A. P. 2019. Delineating the contribution of
1297 Spc105-bound PP1 to spindle checkpoint silencing and kinetochore microtubule attachment
1298 regulation. *J Cell Biol,* 218**,** 3926-3942.

1299 SALIC, A., WATERS, J. C. & MITCHISON, T. J. 2004. Vertebrate shugoshin links sister centromere
1300 cohesion and kinetochore microtubule stability in mitosis. *Cell,* 118**,** 567-78.

1301 SANE, A., SRIDHAR, S., SANYAL, K. & GHOSH, S. K. 2021. Shugoshin ensures maintenance of the spindle
1302 assembly checkpoint response and efficient spindle disassembly. *Mol Microbiol,* 116**,** 1079-
1303 1098.

1304 SANTAGUIDA, S., VERNIERI, C., VILLA, F., CILIBERTO, A. & MUSACCHIO, A. 2011. Evidence that Aurora
1305 B is implicated in spindle checkpoint signalling independently of error correction. *EMBO J,* 30**,**
1306 1508-19.

1307 SAURIN, A. T., VAN DER WAAL, M. S., MEDEMA, R. H., LENS, S. M. & KOPS, G. J. 2011. Aurora B
1308 potentiates Mps1 activation to ensure rapid checkpoint establishment at the onset of mitosis.
1309 *Nat Commun,* 2**,** 316.

1310 SCHINDELIN, J., ARGANDA-CARRERAS, I., FRISE, E., KAYNIG, V., LONGAIR, M., PIETZSCH, T., PREIBISCH,
1311 S., RUEDEN, C., SAALFELD, S., SCHMID, B., TINEVEZ, J. Y., WHITE, D. J., HARTENSTEIN, V.,
1312 ELICEIRI, K., TOMANCAK, P. & CARDONA, A. 2012. Fiji: an open-source platform for biological-
1313 image analysis. *Nat Methods,* 9**,** 676-82.

1314 SIEVERS, F., WILM, A., DINEEN, D., GIBSON, T. J., KARPLUS, K., LI, W., LOPEZ, R., MCWILLIAM, H.,
1315 REMMERT, M., SODING, J., THOMPSON, J. D. & HIGGINS, D. G. 2011. Fast, scalable generation
1316 of high-quality protein multiple sequence alignments using Clustal Omega. *Mol Syst Biol,* 7**,**
1317 539.

1318 SIONOV, E., LEE, H., CHANG, Y. C. & KWON-CHUNG, K. J. 2010. Cryptococcus neoformans overcomes
1319 stress of azole drugs by formation of disomy in specific multiple chromosomes. *PLoS Pathog,*
1320 6**,** e1000848.

1321 SRIDHAR, S., HORI, T., NAKAGAWA, R., FUKAGAWA, T. & SANYAL, K. 2021. Bridgin connects the outer
1322 kinetochore to centromeric chromatin. *Nat Commun,* 12**,** 146.

1323 SUDAKIN, V., CHAN, G. K. & YEN, T. J. 2001. Checkpoint inhibition of the APC/C in HeLa cells is mediated
1324 by a complex of BUBR1, BUB3, CDC20, and MAD2. *J Cell Biol,* 154**,** 925-36.

1325 SUTRADHAR, S., YADAV, V., SRIDHAR, S., SREEKUMAR, L., BHATTACHARYYA, D., GHOSH, S. K., PAUL,
1326 R. & SANYAL, K. 2015. A comprehensive model to predict mitotic division in budding yeasts.
1327 *Mol Biol Cell,* 26**,** 3954-65.

1328 TANAKA, T. U., RACHIDI, N., JANKE, C., PEREIRA, G., GALOVA, M., SCHIEBEL, E., STARK, M. J. &
1329 NASMYTH, K. 2002. Evidence that the Ipl1-Sli15 (Aurora kinase-INCENP) complex promotes
1330 chromosome bi-orientation by altering kinetochore-spindle pole connections. *Cell,* 108**,** 317-
1331 29.

1332 TASHIRO, S., HANDA, T., MATSUDA, A., BAN, T., TAKIGAWA, T., MIYASATO, K., ISHII, K., KUGOU, K.,
1333 OHTA, K., HIRAOKA, Y., MASUKATA, H. & KANOH, J. 2016. Shugoshin forms a specialized
1334 chromatin domain at subtelomeres that regulates transcription and replication timing. *Nat*
1335 *Commun,* 7**,** 10393.

1336 TATCHELL, K., MAKRANTONI, V., STARK, M. J. & ROBINSON, L. C. 2011. Temperature-sensitive ipl1-
1337 2/Aurora B mutation is suppressed by mutations in TOR complex 1 via the Glc7/PP1
1338 phosphatase. *Proc Natl Acad Sci U S A,* 108**,** 3994-9.

1339 VAN HOOFF, J. J., TROMER, E., VAN WIJK, L. M., SNEL, B. & KOPS, G. J. 2017. Evolutionary dynamics of
1340 the kinetochore network in eukaryotes as revealed by comparative genomics. *EMBO Rep,* 18**,**
1341 1559-1571.

1342 VANOOSTHUYSE, V. & HARDWICK, K. G. 2009. A novel protein phosphatase 1-dependent spindle
1343 checkpoint silencing mechanism. *Curr Biol,* 19**,** 1176-81.

1344 VANOOSTHUYSE, V., PRYKHOZHIJ, S. & HARDWICK, K. G. 2007. Shugoshin 2 regulates localization of
1345 the chromosomal passenger proteins in fission yeast mitosis. *Mol Biol Cell,* 18**,** 1657-69.

1346 VARSHNEY, N., SOM, S., CHATTERJEE, S., SRIDHAR, S., BHATTACHARYYA, D., PAUL, R. & SANYAL, K.
1347 2019. Spatio-temporal regulation of nuclear division by Aurora B kinase Ipl1 in Cryptococcus
1348 neoformans. *PLoS Genet,* 15**,** e1007959.

1349 VERZIJLBERGEN, K. F., NERUSHEVA, O. O., KELLY, D., KERR, A., CLIFT, D., DE LIMA ALVES, F.,
1350 RAPPSILBER, J. & MARSTON, A. L. 2014. Shugoshin biases chromosomes for biorientation
1351 through condensin recruitment to the pericentromere. *Elife,* 3**,** e01374.

1352 WANG, X., YANG, Y., DUAN, Q., JIANG, N., HUANG, Y., DARZYNKIEWICZ, Z. & DAI, W. 2008. sSgo1, a
1353 major splice variant of Sgo1, functions in centriole cohesion where it is regulated by Plk1. *Dev*
1354 *Cell,* 14**,** 331-41.

1355 WATERHOUSE, A. M., PROCTER, J. B., MARTIN, D. M., CLAMP, M. & BARTON, G. J. 2009. Jalview
1356 Version 2--a multiple sequence alignment editor and analysis workbench. *Bioinformatics,* 25**,**
1357 1189-91.

1358 WU, F., AKBAR, H., WANG, C., YUAN, X., DOU, Z., MULLEN, M., NIU, L., ZHANG, L., ZANG, J., WANG, Z.,
1359 YAO, X., SONG, X. & LIU, X. 2024. Sgo1 interacts with CENP-A to guide accurate chromosome
1360 segregation in mitosis. *J Mol Cell Biol,* 15.

1361 XU, Z., CETIN, B., ANGER, M., CHO, U. S., HELMHART, W., NASMYTH, K. & XU, W. 2009. Structure and
1362 function of the PP2A-shugoshin interaction. *Mol Cell,* 35**,** 426-41.

1363 YADAV, V. & SANYAL, K. 2018. Sad1 Spatiotemporally Regulates Kinetochore Clustering To Ensure
1364 High-Fidelity Chromosome Segregation in the Human Fungal Pathogen Cryptococcus
1365 neoformans. *mSphere,* 3.

1366 YAMAGISHI, Y., SAKUNO, T., SHIMURA, M. & WATANABE, Y. 2008. Heterochromatin links to
1367 centromeric protection by recruiting shugoshin. *Nature,* 455**,** 251-5.

1368 ZICH, J. & HARDWICK, K. G. 2010. Getting down to the phosphorylated 'nuts and bolts' of spindle
1369 checkpoint signalling. *Trends Biochem Sci,* 35**,** 18-27.

Figures

Figure 1. *Polisetty et. al*

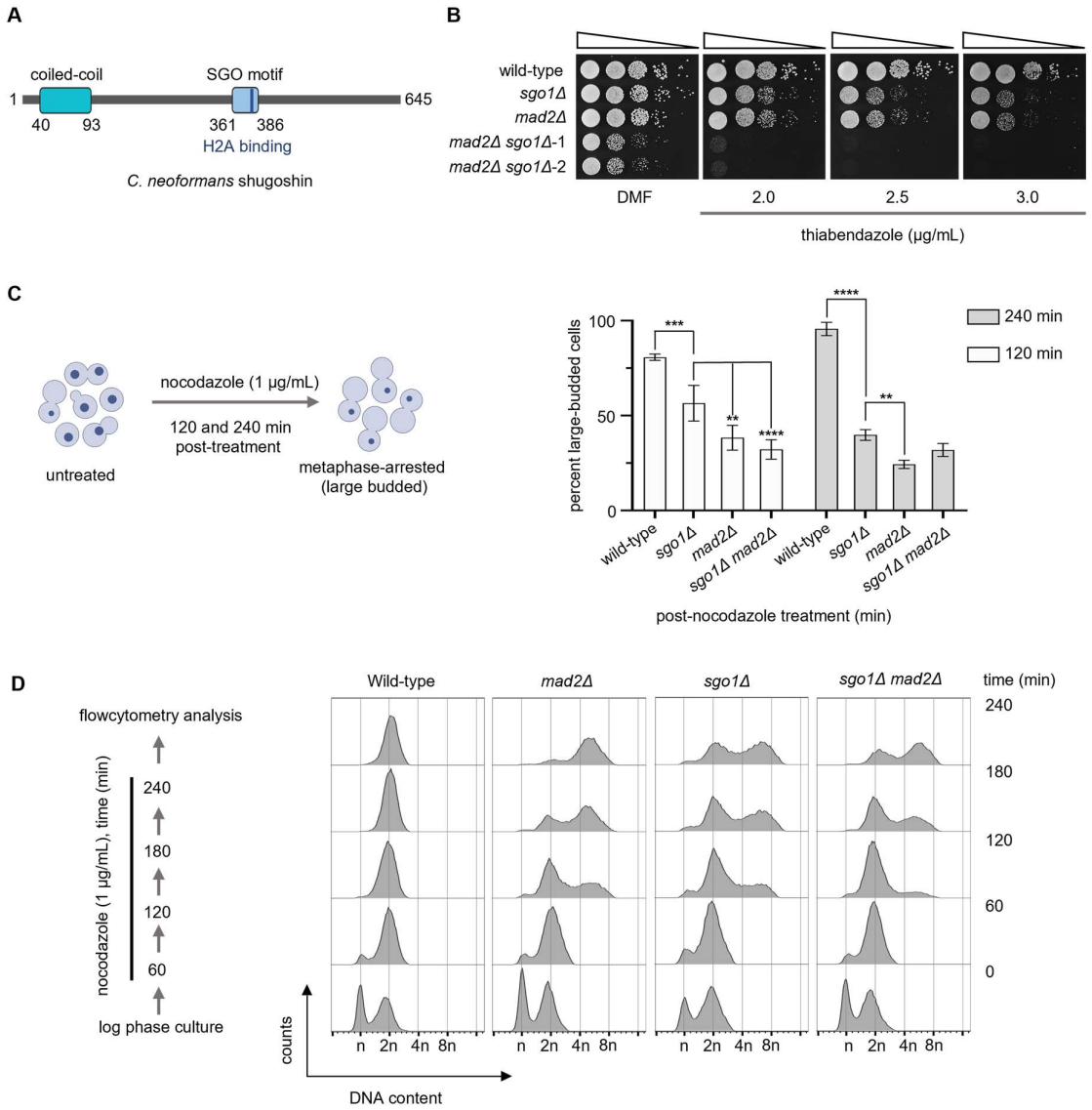

Figure 1. Shugoshin is required for a robust spindle assembly checkpoint arrest. (A) Schematic of the predicted motifs present in Sgo1 of *C. neoformans*. **(B)** A ten-fold serial dilution spotting assay to score for the sensitivity of strains CNVY108 (*SGO1 GFP-H4*), CNSD110 (*GFP-H4 sgo1Δ*), SHR741 (*GFP-H4 mad2Δ*), CNSD148 (*GFP-H4 sgo1Δ mad2Δ*) on plates containing the indicated concentrations of thiabendazole (TBZ). No drug represents DMF (dimethyl formamide) only. The plates were incubated at 30°C for 24 h. **(C)** *Left,* schematic of the assay to score for cell cycle arrest phenotypes when treated with nocodazole. Cells treated with nocodazole for 120 and 240 min were scored for cell cycle arrest phenotypes. *Right,* bar graphs representing

1379 the proportion of large-budded cells in the indicated strains, N=3, n>100, cells counted
1380 in each experiment. Two-way ANOVA with Tukey's multiple comparison test was used
1381 to estimate the significance. ****p<0.0001, ***p<0.001, **p=0.0019/0.0072. Non-
1382 significant p-values were omitted from the graph. **(D)** *Left*, an outline of the assay to
1383 study the effect of nocodazole on the ploidy content of indicated strains using flow
1384 cytometry. *Right*, histograms depicting ploidy changes associated with nocodazole
1385 treatment.

Figure 2. *Polisetty et. al*

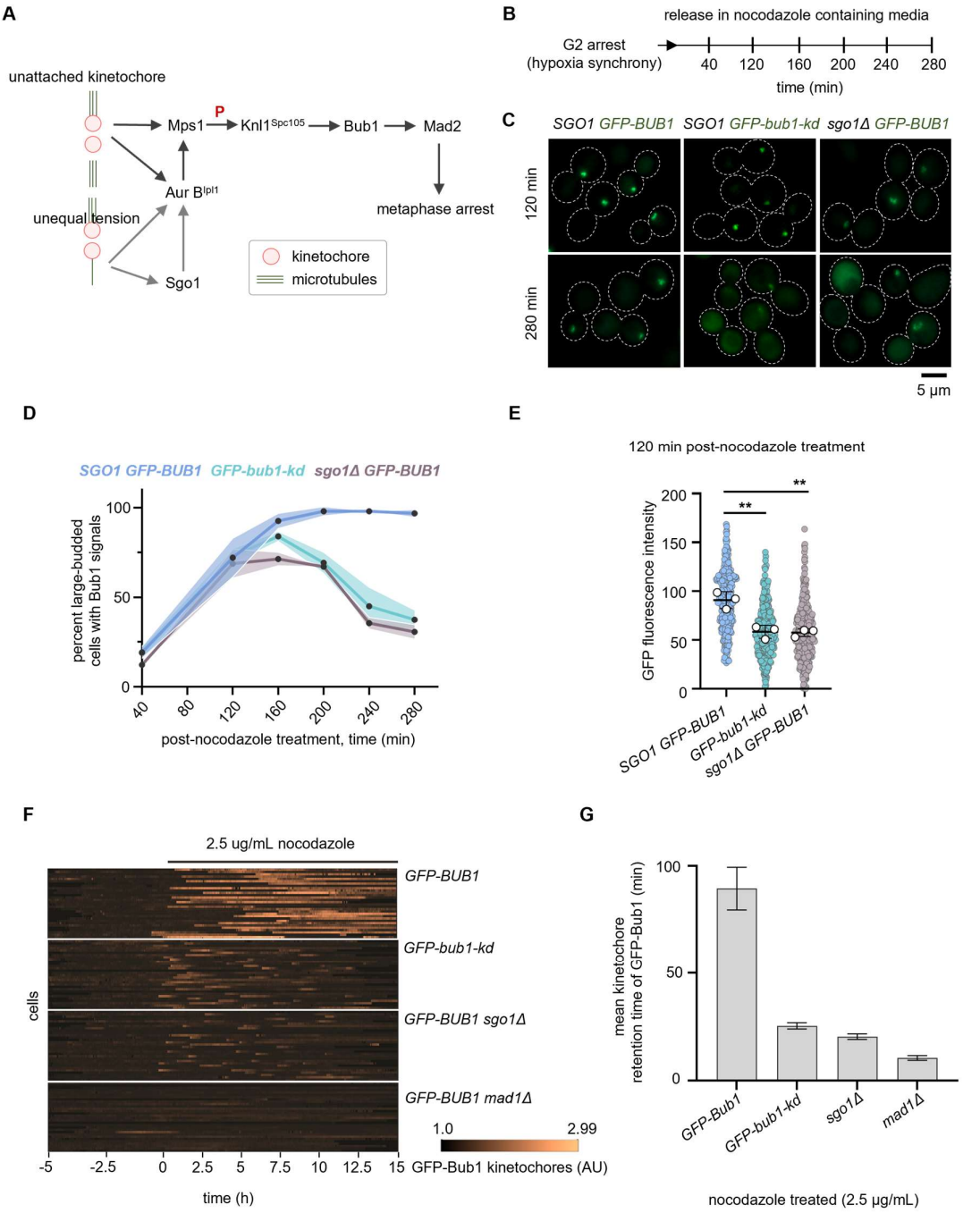

Figure 2. Shugoshin ensures Bub1 is retained at kinetochores to maintain the spindle assembly checkpoint arrest. (A) Schematic of the SAC pathway and the evolutionarily conserved role of Sgo1 and Aurora B^{Ipl1} in detecting erroneous kinetochore-MT attachments. **(B)** An experimental workflow followed to determine the GFP-Bub1 localization dynamics under nocodazole-treated conditions. **(C)** Sub-

1391 cellular localization of GFP-Bub1 localization in IL102 (*SGO1*), IL143 (*bub1-kd*) and
1392 CNSD176 (*sgo1Δ*). For representation, cells treated with nocodazole for 120 and 280
1393 min were shown. Scale bar, 5 μm. **(D)** Quantification of the proportion of large-budded
1394 cells with GFP-Bub1 signal in indicated strains treated with nocodazole. N=3, n>100
1395 cells were analyzed, and the shaded regions above and below the line graphs
1396 represent error bands corresponding to SD. **(E)** Quantification of GFP-Bub1
1397 fluorescence intensity values at 120 min post-nocodazole treatment. N=3, n>100 cells
1398 analyzed for each experiment. White circles represent the average intensity values of
1399 replicates. A mean of the average intensity values of replicates is represented as a
1400 black bar, and error bars represent SD. An unpaired t-test was used to test the
1401 significance, ** p=0.0092, ns =0.1131 **(F)** Microfluidics assays to determine the
1402 retention time of GFP-Bub1 at kinetochores in response to nocodazole treatment.
1403 Temporal heat maps of 30 randomly selected cells are shown. The heat map
1404 represents the changes in kinetochore localization signal of GFP-Bub1 over time.
1405 Each bright track on the *y*-axis of the heat map represents GFP-Bub1 signals from an
1406 individual cell (median of the brightest 5 pixels in each cell divided by the overall cell
1407 median brightness). The length of each bright track along the *x*-axis represents the
1408 time (min). The time of addition of nocodazole (2.5 μg/mL) is considered as 0 h.
1409 Images are taken every 2 min for 15 h. Assays were performed using strains IL102
1410 (*GFP-BUB1*), IL143 (*GFP-bub1-kd*), CNSD176 (*GFP-BUB1 sgo1Δ*), and IL089 (*GFP-*
1411 *BUB1 mad1Δ*) strains. **(G)** Bar graphs representing the quantitative analysis of the
1412 GFP-Bub1 retention time at kinetochores obtained from microfluidics assays in the
1413 above-indicated strains. n=30, error bars represent SEM.

Figure 3. *Polisetty et. al*

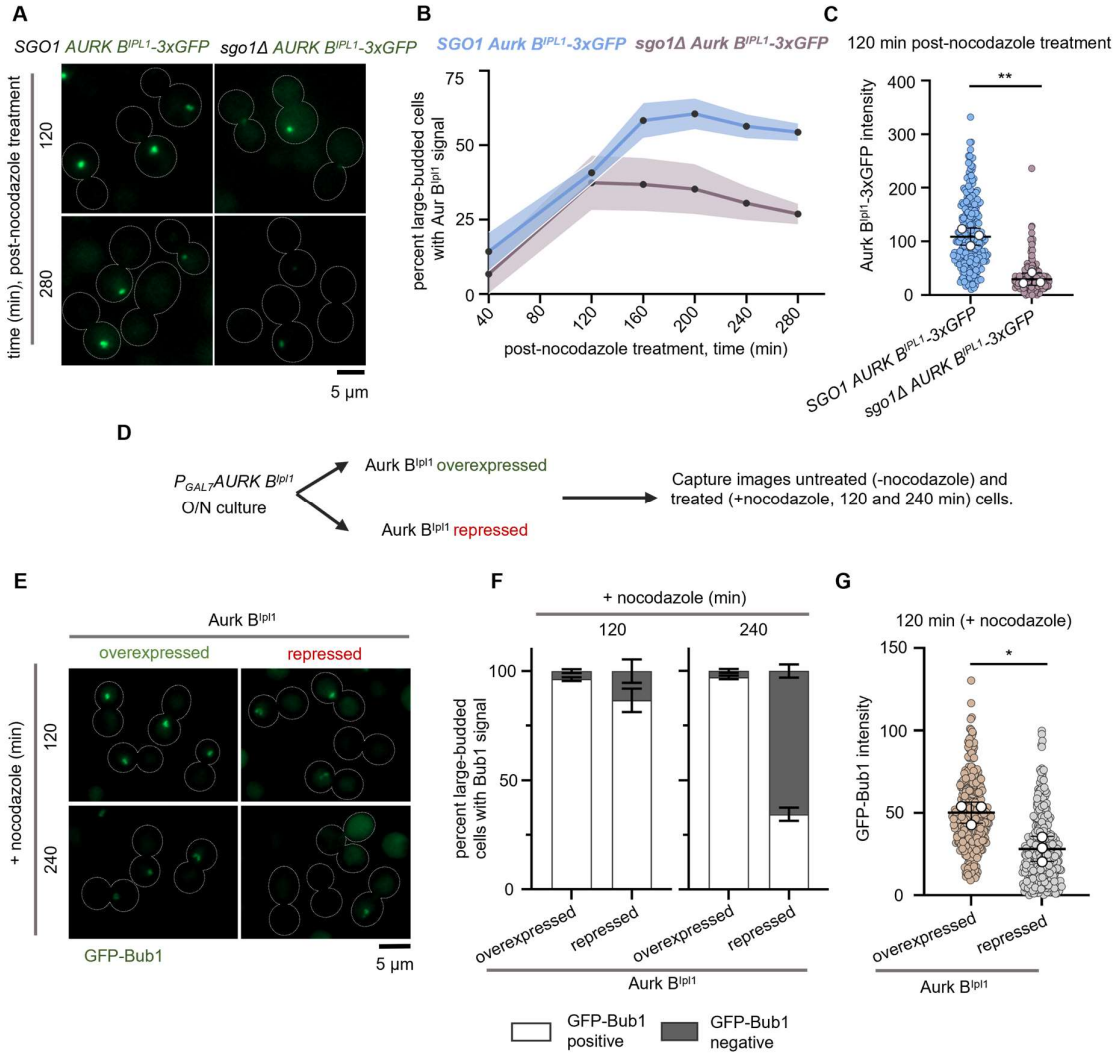

Figure 3. Shugoshin-dependent Aurora B^{Ipl1} pool at kinetochores ensures maintenance of Bub1 to prolong the checkpoint arrest. (A) Sub-cellular localization of Aurora B^{Ipl1}-3xGFP localization in CNSD190 (*AURORA B^{Ipl1}-3xGFP mCherry-CENP-A SGO1*) and CNSD196 (*AURORA B^{Ipl1}-3xGFP mCherry-CENP-A sgo1Δ*) strains treated with nocodazole. For representation, cells treated with nocodazole for 120 and 280 min were shown. Scale bar, 5µm. **(B)** Quantification of the proportion of large-budded cells with Aurora B^{Ipl1}-3xGFP signals in the indicated strains. N=3, n>100 cells were analyzed, and the shaded regions above and below the line graph represent error bands corresponding to SD. **(C)** Quantification of Aurora B^{Ipl1}-3xGFP fluorescence intensity values at 120 min post-nocodazole treatment. N=3, n>58 cells for each experiment. White circles represent the average intensity values of replicates. The mean of the average intensity values of replicates is represented as

1426 a black bar. Error bars represent SD. An unpaired t-test was used to test the
1427 significance, ** p= 0.0013. **(D)** Schematic to assess the response of Aurora B^{Ipl1}
1428 (over)expression or depletion to nocodazole treatment. **(E)** Sub-cellular localization of
1429 GFP-Bub1 localization in CNSD205 (*GAL7-3xFLAG-AURORA B^{IPL1} GFP-BUB1*)
1430 Aurora B^{Ipl1} (over)expressed and repressed conditions treated with nocodazole. Cells
1431 treated with nocodazole for 120 and 240 min are shown for representation. Scale bar,
1432 5 µm. **(F)** Bar graphs representing the proportion of large-budded cells with or without
1433 of GFP-Bub1 signals at 120 and 240 min of nocodazole treatment. N=3, n>100 cells
1434 analyzed for each experiment. Error bars represent SD. **(G)** Quantification of GFP-
1435 Bub1 fluorescence intensity values in Aurora B^{Ipl1} (over)expressed and repressed
1436 conditions at 120 min of nocodazole treatment. White circles represent the average
1437 intensity values of replicates. The mean of the average intensity values of the
1438 replicates is represented as a black bar. Error bars represent SD. N=3, n> 79 cells
1439 analyzed for each experiment. An unpaired t-test was used to test the significance,
1440 *p=0.0439.

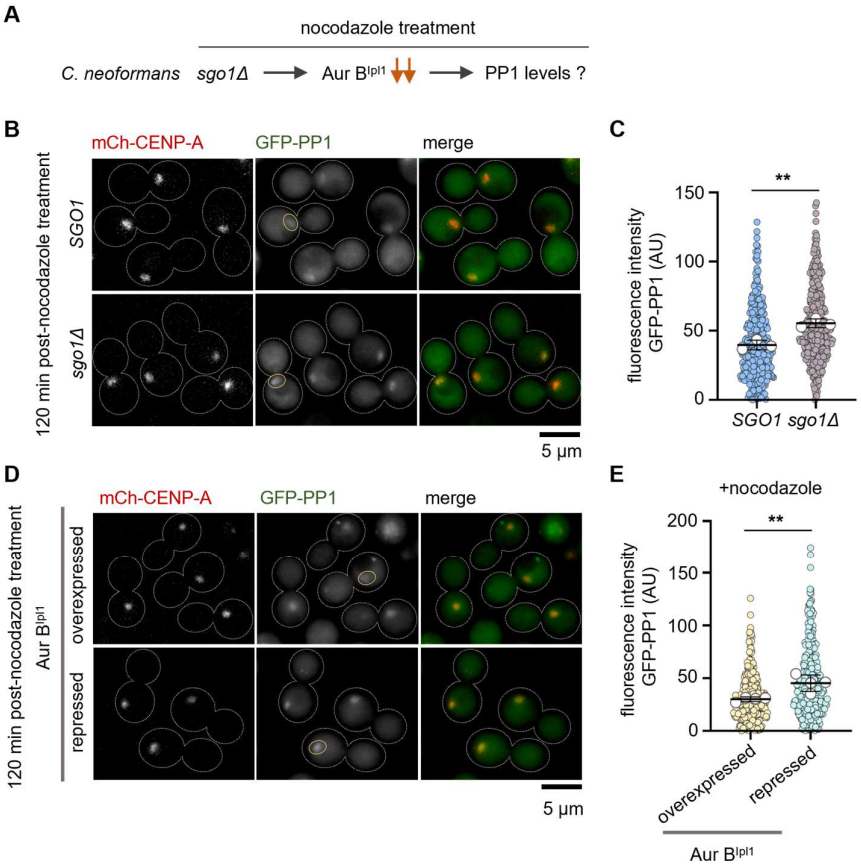

Figure 4. Sgo1-mediated Aurora B^{Ipl1} recruitment prevents excess PP1 phosphatase at the kinetochore. (A) The effect of *sgo1Δ* on maintaining a balance between Aurora B^{Ipl1} and PP1 levels at kinetochore in *C. neoformans*. **(B)** Sub-cellular localization of CNKB003 (*GFP-PP1 mCherry-CENP-A SGO1*) and CNSD180 (*GFP-PP1 mCherry-CENP-A sgo1Δ*) cells treated with nocodzole (1 µg/mL) for 120 min. Yellow ovals highlight PP1-GFP signals. **(C)** Quantification of GFP-PP1 fluorescence signal intensity values in the indicated strains treated with nocodazole. N=3, n>100 cells were analyzed for each experiment. White circles represent the average GFP-PP1 signal intensities calculated for each experimental repeat. An unpaired t-test was used to determine statistical significance. **p= 0.0044. The mean of the average intensity values of replicates is represented as a black bar. Error bars represent SD. **(D)** Microscopic images of CNKB023 (*GFP-PP1 mCherry-CENP-A GAL7-3xFLAG AURORA B^{IPL1}*) Aurora B^{Ipl1} (over)expressed and repressed conditions treated with nocodazole (1 µg/mL) for 120 min. **(E)** Quantification of fluorescence intensity values of GFP-PP1 signals in conditions mentioned above. N=4, n=100 cells for each

experiment. White circles represent the average intensity values of replicates. Error bars represent SD. The mean of the average intensity values plotted is represented as a black bar. Paired t-test was used to determine statistical significance. **p= 0.0069.

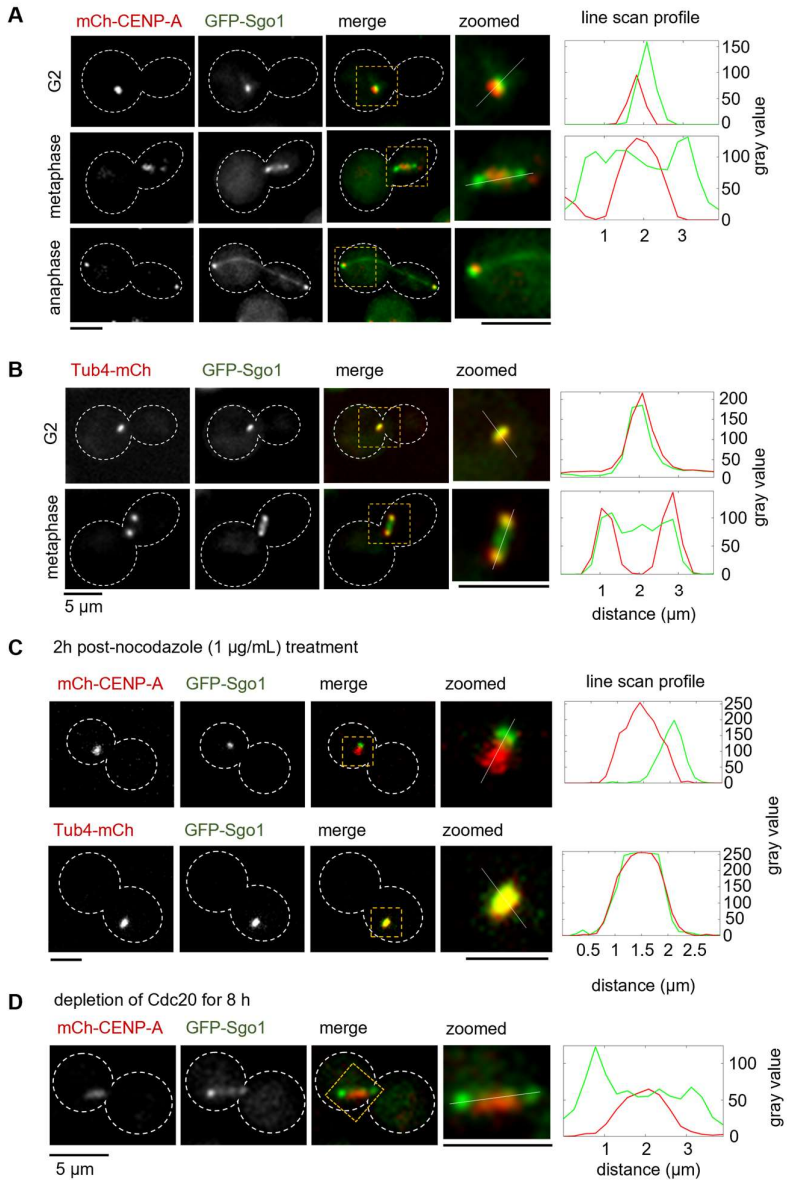

Figure 5. ***Polisetty et. al***

Figure 5. Kinetochore proximal association of Sgo1 in MT-depolymerizing conditions. (A-D) *Left,* microscopic images of GFP-Sgo1 localized with a kinetochore marker, CENP-A, and an SPB marker, Tub4, at different stages of the mitotic cell cycle, in nocodazole treated and Cdc20 depleted conditions. Scale bar, 5 µm. **(A)** CNSD125 (*GFP-SGO1 mCherry-CENP-A*). **(B)** CNSD130 (*GFP-SGO1 TUB4-mCherry*). **(C)** Nocodazole (1 µg/mL) treated condition. *Top panel*, CNSD125. *Bottom panel*, CNSD130. **(D)** Cdc20 depletion condition, CNSD167 (*GFP-SGO1 mCherry-CENP-A GAL7-3xFLAG-CDC20*). *Right*, line scan profiles of both GFP (Sgo1) and mCherry (CENP-A, Tub4) fluorescence signals. Distance plotted on the *x*-axis

1468 represents the length of the line drawn on the image to measure fluorescence
1469 intensity. Gray values on the *y*-axis represent the fluorescence signal intensities.

Figure 6. *Polisetty et. al*

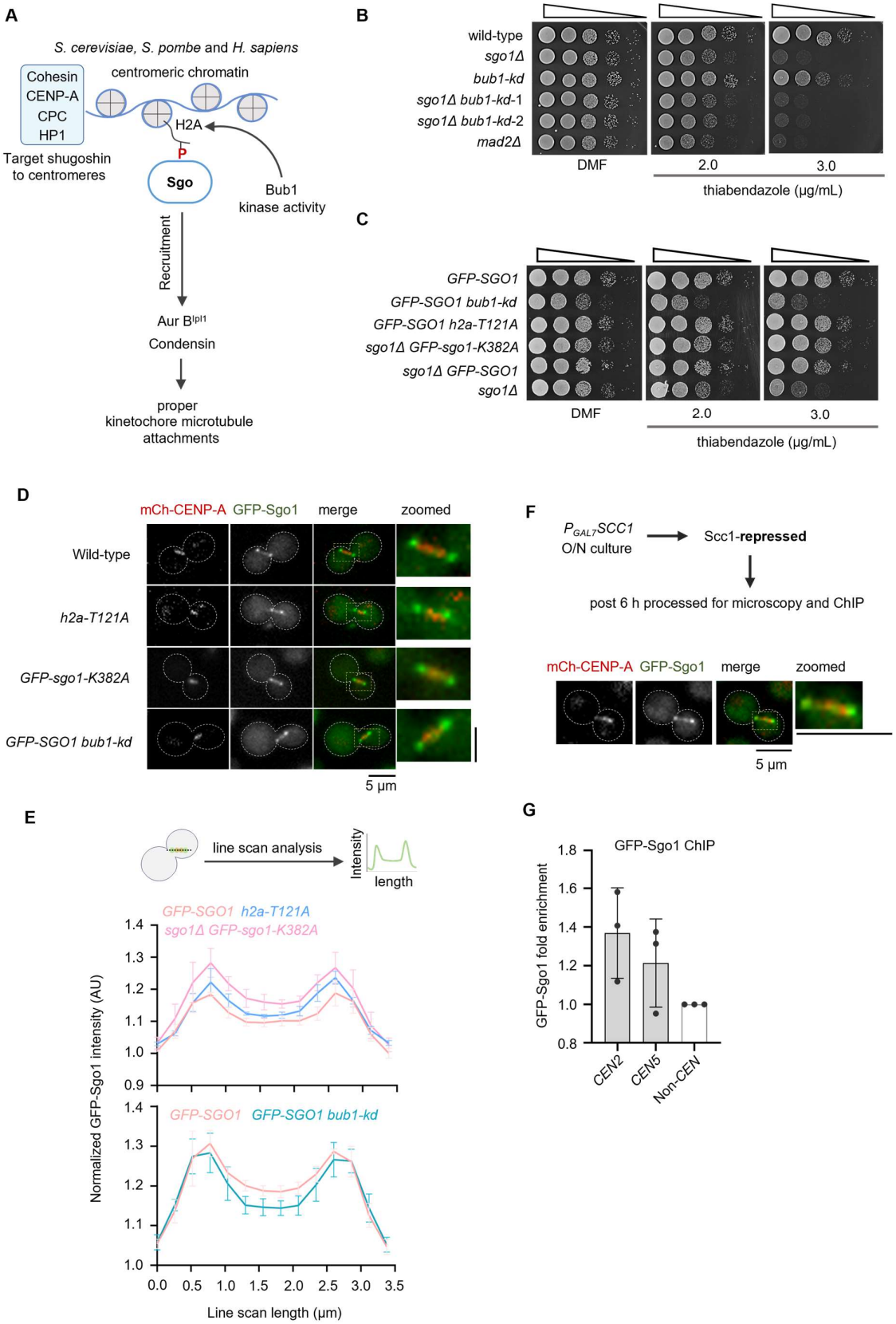

1470 **Figure 6. The kinase activity of Bub1 is dispensable for shugoshin-mediated**
1471 **maintenance of the spindle assembly checkpoint. (A)** Schematic of the conserved
1472 pathway of shugoshin recruitment to kinetochores. **(B)** A ten-fold serial dilution
1473 spotting assay to score for the sensitivity of the CNSD110 (*sgo1Δ*), IL143 (*GFP-bub1-*
1474 *kd*), CNSD173 (*sgo1Δ GFP-bub1-kd*) double mutants and SHR866 (*mad2Δ*) to
1475 thiabendazole. **(C)** A ten-fold serial dilution spotting assay to score for the sensitivity
1476 of the CNSD125 (*GFP-SGO1 mCherry-CENP-A*), CNSD215 (*GFP-SGO1 mCherry-*
1477 *CENP-A bub1-kd-3XFLAG*), CNSD219 (*GFP-SGO1 mCherry-CENP-A h2a-T121A*),
1478 CNSD218 (*sgo1Δ GFP-sgo1-K382A-SH1 mCherry-CENP-A*), CNSD207 (*sgo1Δ*
1479 *GFP-SGO1-SH1*) and CNSD110 (*sgo1Δ*). **(D)** Microscopic images of GFP-Sgo1
1480 localized with CENP-A at metaphase stage in wild-type and mutant backgrounds.
1481 Scale bar, 5 μm. **(E)** *Top,* Schematic showing the line scan analysis method adopted
1482 to score for the fluorescence intensity of GFP-Sgo1 along the spindle and SPBs.
1483 *Middle,* line scan profile of GFP-Sgo1 in the indicated strains synchronized using
1484 thiabendazole (10 μg/mL) treatment. *Bottom*, line scan profile of GFP-Sgo1 in the
1485 indicated strains synchronized using hypoxia. Distance on the *x*-axis represents the
1486 length of the line drawn on the image to measure fluorescence intensity. The *y*-axis
1487 represent the fluorescence signal intensity values. N=3, n>20 cells were analysed for
1488 each experiment. Each line graph represents mean fluorescence intensity values
1489 calculated from three experimental repeats and error bars represent SD. **(F)** *Top,*
1490 Schematic of the assay used to arrest cells at metaphase by depleting Scc1. *Below*,
1491 microscopic images of GFP-Sgo1 localized with CENP-A metaphase in Scc1 depleted
1492 conditions. **(G)** Fold enrichment of Sgo1 at kinetochores in metaphase arrested cell
1493 obtained by cross-linking chromatin immunoprecipitation (ChIP) followed by
1494 quantitative polymerase chain reaction (qPCR). *CEN2* and *CEN5* represent
1495 centromeres 2 and 5, non-CEN region represents *LEU2* locus. N=3, and error bars
1496 represent SD.

Supplementary Figures

Supplementary Figure 1. *Polisetty et. al*

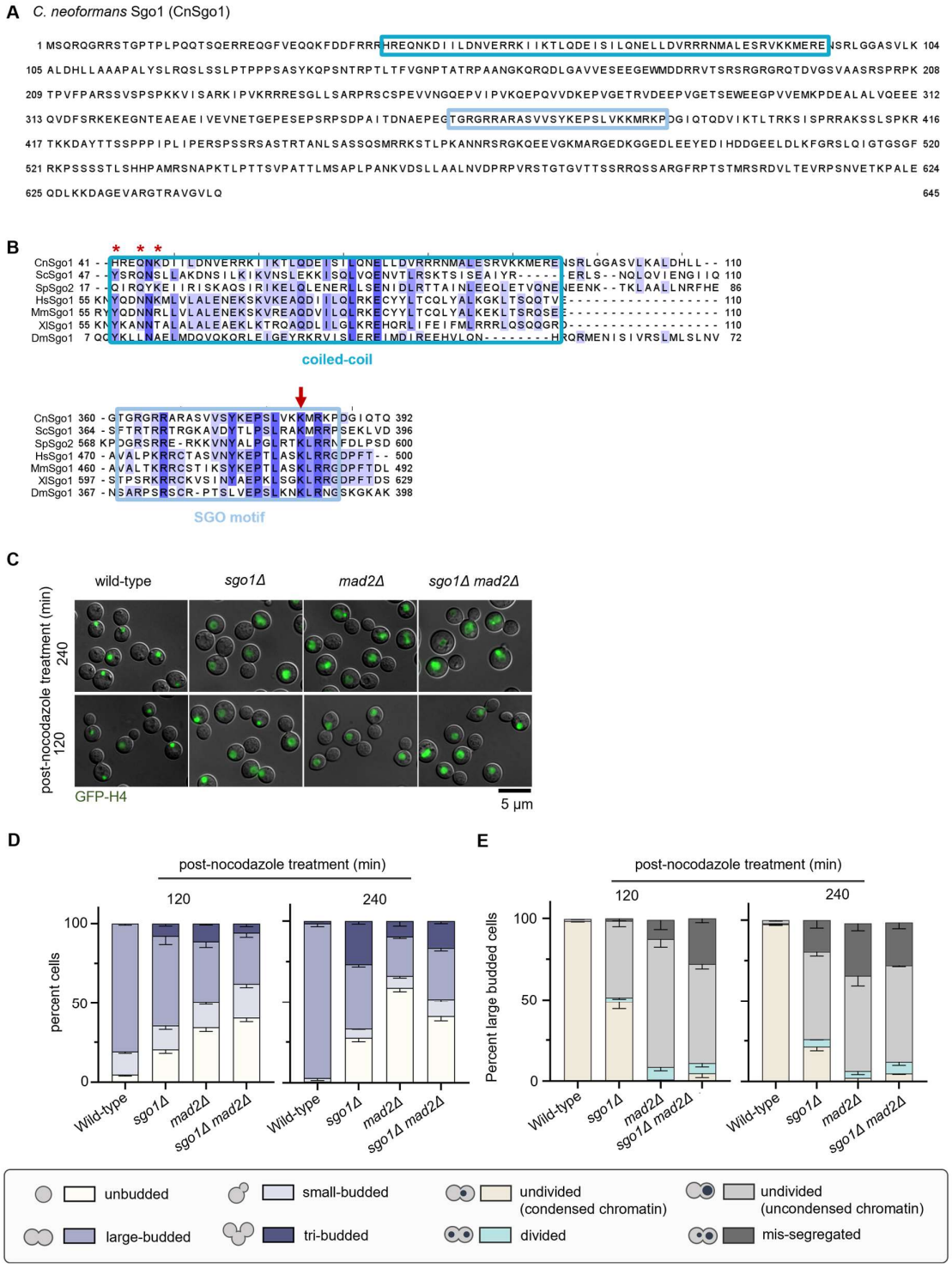

Supplementary Figure 1. *C. neoformans* Sgo1, carrying a conserved coiled-coil domain and the SGO motif, is required to maintain SAC arrest in nocodazole-treated cells. (A) The protein sequence of *C. neoformans* Sgo1. **(B)** Multiple sequence alignment (MSA) of the

1500 CnSgo1 N-terminal coiled-coil and the C-terminal SGO motif with vertebrate and invertebrate
1501 species (Cn- *C. neoformans*; Sc- *Saccharomyces cerevisiae*; Sp- *Schizosaccharomyces*
1502 *pombe*; Hs- *Homo sapiens*; Mm- *Mus musculus*; Xl- *Xenopus laevis*; Dm- *Drosophila*
1503 *melanogaster*). Multiple sequence alignment of Sgo1 homologs was performed using Clustal
1504 Omega (Sievers et al., 2011), and the alignment was formatted using Jalview 2 (Waterhouse
1505 et al., 2009). *Represent amino acid residues involved in PP2A binding. The dark blue circle
1506 represents the key residue (K382 in *C. neoformans*) required for Bub1-mediated kinetochore
1507 proximal centromere localization of shugoshin. The teal blue colored box represents the
1508 coiled-coil domain. The light blue colored box represents the conserved basic SGO motif. **(C)**
1509 Microscopic images of GFP-H4 in CNVY108 (*SGO1 MAD2*), CNSD117 (*sgo1Δ*), SHR866
1510 (*mad2Δ*), CNSD148 (*sgo1Δ mad2Δ*) treated with nocodazole (1 µg/mL) for 120- and 240-min.
1511 Scale bar, 5 µm. **(D)** Bar graphs representing the proportion of unbudded, small-budded,
1512 large-budded, and tri-budded cells. N=3, n>100 cells counted in each experiment. **(E)** Bar
1513 graphs representing the proportion of large-budded cells of indicated phenotypes, N=3, n>100
1514 cells counted in each experiment.

1515

1516

1517

1518

1519

1520

1521

1522

1523

Supplementary Figure 2. *Polisetty et. al*

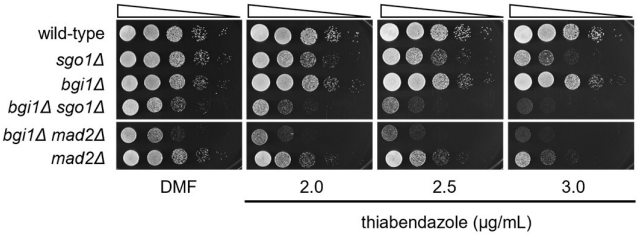

1524 **Supplementary Figure 2. *sgo1Δ bgi1Δ* double mutant cells exhibit enhanced sensitivity**
1525 **to MT depolymerizing drug.** A ten-fold serial dilution spotting assay to score for the sensitivity
1526 of the wild-type CNVY108 (*SGO1 BGI1 GFP-H4*), CNSD117 (*sgo1Δ GFP-H4)*, SHR741
1527 (*mad2Δ GFP-H4*), SHR830 (*bgi1Δ GFP-H4*), CNSD148 (*sgo1Δ mad2Δ GFP-H4*) and
1528 CNSD163 (*sgo1Δ bgi1Δ GFP-H4*) to thiabendazole. No drug represents DMF (Dimethyl
1529 formamide) only. The plates were incubated at 30°C for 24 h.

Supplementary Figure 3. ***Polisetty et. al***

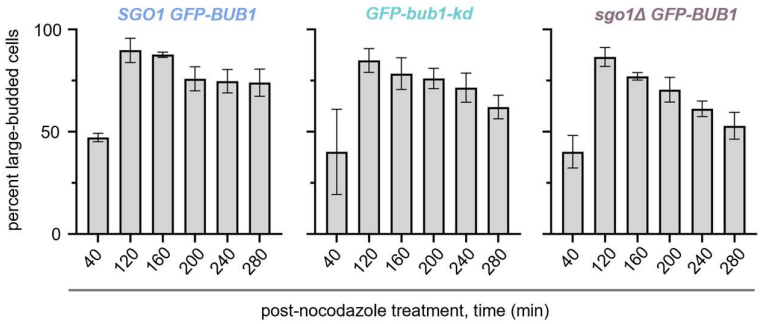

Supplementary Figure 3. The proportion of large-budded cells scored for the presence or absence of GFP-Bub1 signal post nocodazole treatment. Bar graphs representing the proportion of large-budded cells obtained post nocodazole treatment in the indicated strains, N=3, n>100, cells counted in each experiment. Errors bars represent SD.

Supplementary Figure 4. *Polisetty et. al*

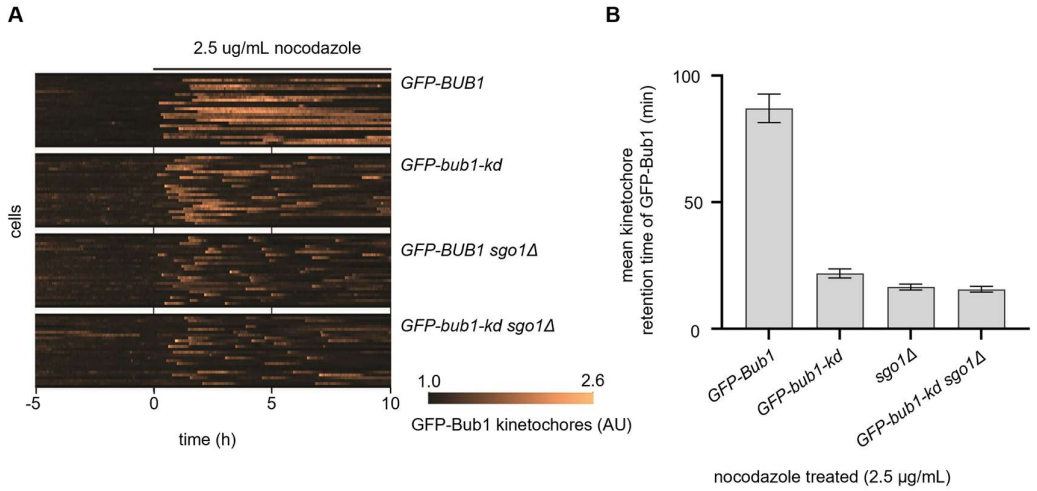

Supplementary Figure 4. *bub1-kd sgo1Δ* double mutant cells behave similar to single *sgo1Δ* mutant cells. (A) Microfluidics assay to determine the retention time of GFP-Bub1 at kinetochores in response to nocodazole treatment. Temporal heat maps of 30 randomly selected cells are shown. The heat map represents the changes in the kinetochore localization signal of GFP-Bub1 over time. Each bright track on the *y*-axis of the heat map represents GFP-Bub1 signals from an individual cell (median of the brightest 5 pixels in each cell divided by the overall cell median brightness). The length of each bright track along the *x*-axis represents the time (min). The time of addition of nocodazole (2.5 µg/mL) is considered as 0 hr. Images are taken every 2 min for 10 h. Assay was performed using IL102 (*GFP-BUB1*), IL143 (*GFP-bub1-kd*), CNSD176 (*GFP-BUB1 sgo1Δ*), and CNSD173 (*GFP-bub1-kd sgo1Δ*) strains. **(B)** Bar graphs representing the quantitative analysis of GFP-Bub1 retention time at kinetochores obtained from microfluidics assays in the above-indicated strains. n=24, error bars represent SEM.

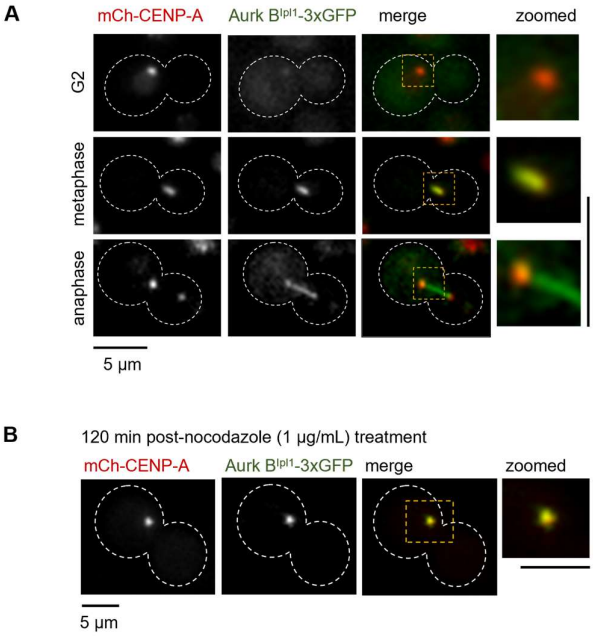

Supplementary Figure 5. Aurora B^{Ipl1} localizes to the kinetochore (CENP-A) during G2 and mitosis and exhibits spindle-like localization. (A) Microscopic images of Aurora B^{Ipl1}-3xGFP localized with a kinetochore protein mCherry-CENP-A at G2, metaphase, and anaphase stages of the cell cycle. **(B)** Colocalization of Aurora B^{Ipl1}-3xGFP with mCherry-CENP-A when treated with nocodazole (1 µg/mL) for 120 min. Scale bar, 5 µm.

Supplementary Figure 6. ***Polisetty et. al***

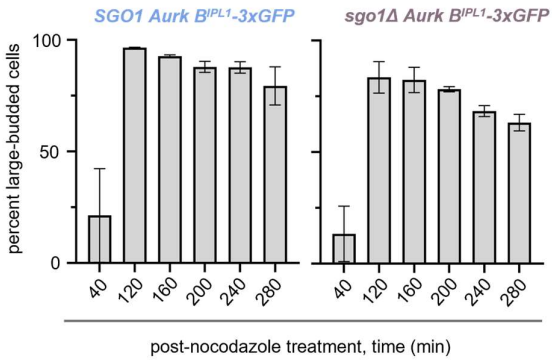

1552 **Supplementary Figure 6. The proportion of large-budded cells scored for the presence**
1553 **or absence of Aurora B^{Ipl1}-3xGFP signal post nocodazole treatment.** Bar graphs
1554 representing the proportion of large-budded cells obtained post nocodazole treatment in the
1555 indicated strains, N=3, n>100, cells counted in each experiment. Errors bars represent SD.

Supplementary Figure 7. ***Polisetty et. al***

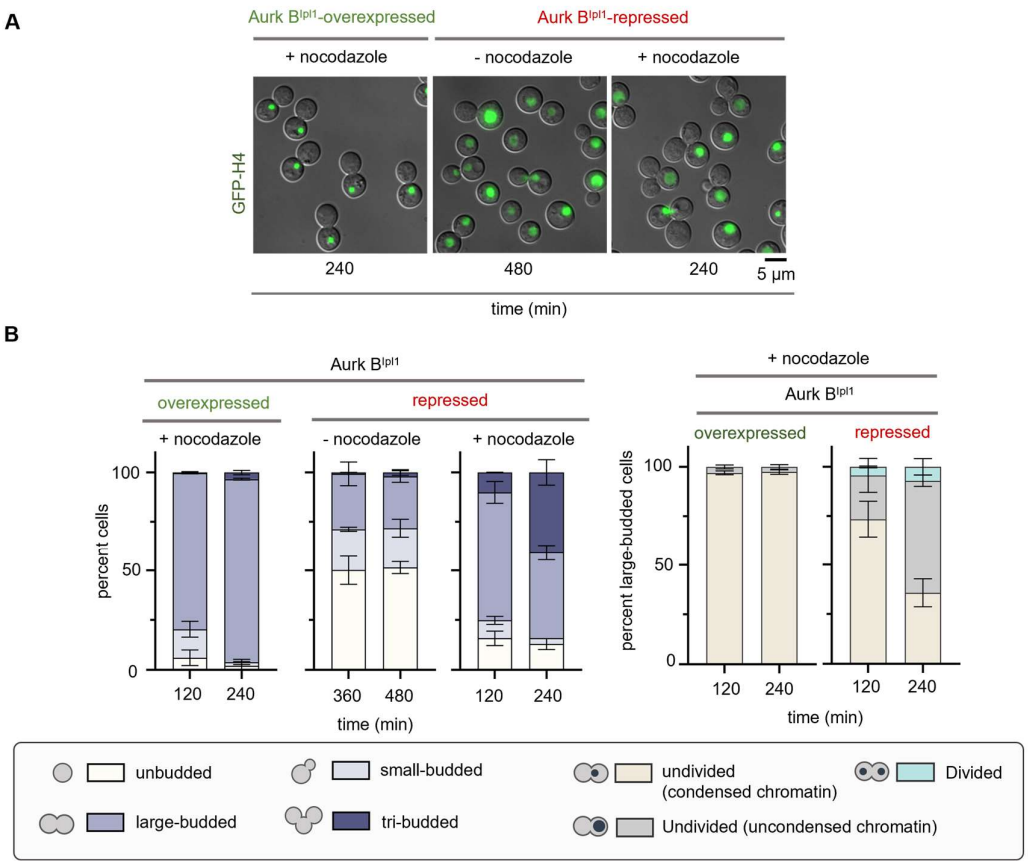

Supplementary Figure 7. Aurora B^{Ipl1} mutants fail to arrest at metaphase in response to nocodazole treatment. (A) Microscopic images of CNNV104 (*GFP-H4 GAL7-AURORA B^{IPL1}*) grown in permissive and non-permissive media in the presence and absence of nocodazole. Scale bar, 5 µm. Representative images of cells treated with nocodazole and depleted of Aurora B^{Ipl1} for 240 and 480 min were shown. **(B)** *Left*, bar graphs representing the proportion of unbudded, small-budded, large-budded, and tri-budded cells. *Right*, bar graphs representing the proportion of large-budded cells of indicated phenotype, N=2, n>100 cells counted for each experiment.

Supplementary Figure 8. ***Polisetty et. al***

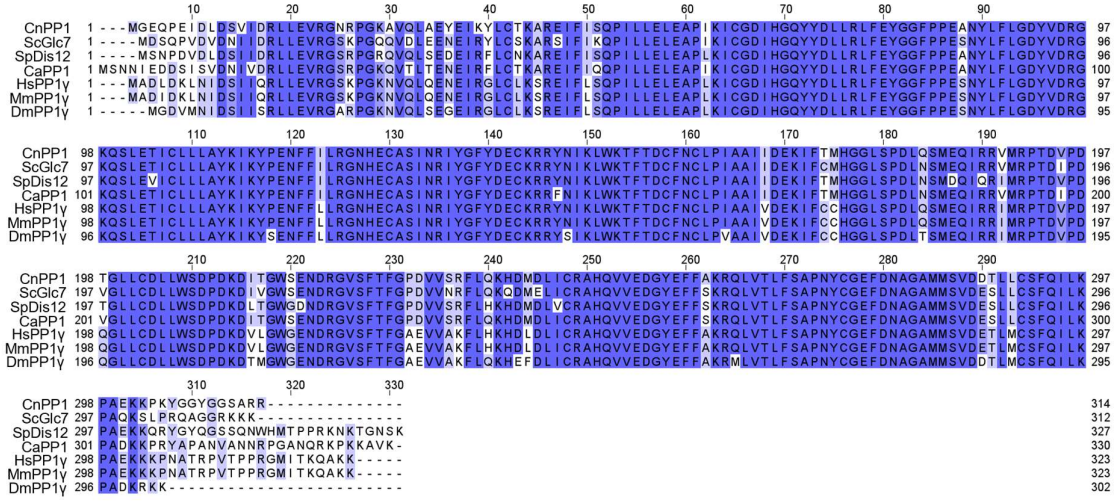

1564 **Supplementary Figure 8. Sequence conservation of *C. neoformans* PP1.** Multiple
1565 sequence alignment of PP1 homolog of *C. neoformans* (CNAG_03706) with vertebrate and
1566 invertebrate species (Cn- *C. neoformans*; Sc- *S. cerevisiae*; Sp- *S. pombe*; Ca- *Candida*
1567 *albicans*; Hs- *H. sapiens*; Mm- *M. musculus*; Dm- *D. melanogaster*) was performed using
1568 Clustal Omega (Sievers et al., 2011) and the alignment was formatted using Jalview 2
1569 (Waterhouse et al., 2009). Highly conserved regions are shaded in dark blue.

Supplementary Figure 9. *Polisetty et. al*

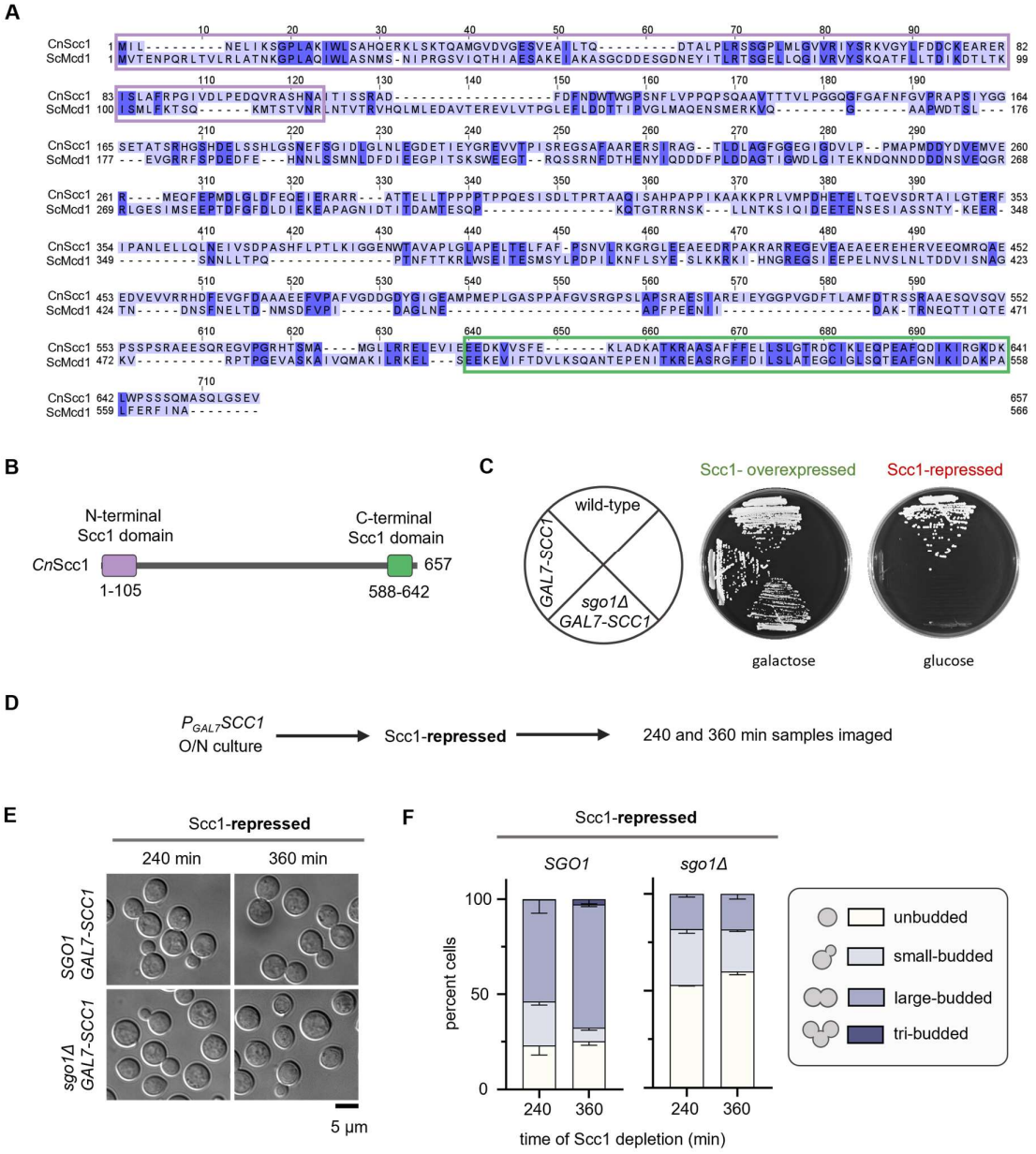

Supplementary Figure 9. Shugoshin responds to tensionless kinetochore-MT attachments. (A) Pairwise sequence alignment of Scc1 homologs of *C. neoformans* (CNAG_01023) and *S. cerevisiae* by Clustal Omega (Sievers et al., 2011), and formatted using Jalview 2 (Waterhouse et al., 2009). Highly conserved regions are shaded in dark blue. The two domains corresponding to N- and C-terminal Scc1 domains (E-values of 2.0e-31 and 2.2e-15, respectively) of CnScc1 are highlighted in violet and green boxes. **(B)** Schematic of the domains present in *C. neoformans* Scc1 protein. **(C)** Plate photographs of strains expressing Scc1 under the regulatable *GAL7* promoter grown in media containing glucose (non-permissive) and galactose (permissive). **(D)** Schematic to check the response of Scc1

1579 repression in *SGO1* and *sgo1Δ* backgrounds. **(E)** Microscopic images of GFP-H4 tagged
1580 CNSD181 (*GAL7-3xFLAG-SCC1*) and CNSD182 (*sgo1Δ GAL7-3xFLAG-SCC1*) strains
1581 depleted of Scc1. Representative images of cells depleted of Scc1 for 4 and 6 h were shown.
1582 Scale bar, 5 μm. **(F)** Bar graphs representing the percentage of unbudded, small-budded,
1583 large-budded, and tri-budded cells scored. N=2, n>100 cells for each experiment, error bars
1584 represent SD.

Supplementary Figure 10. *Polisetty et. al*

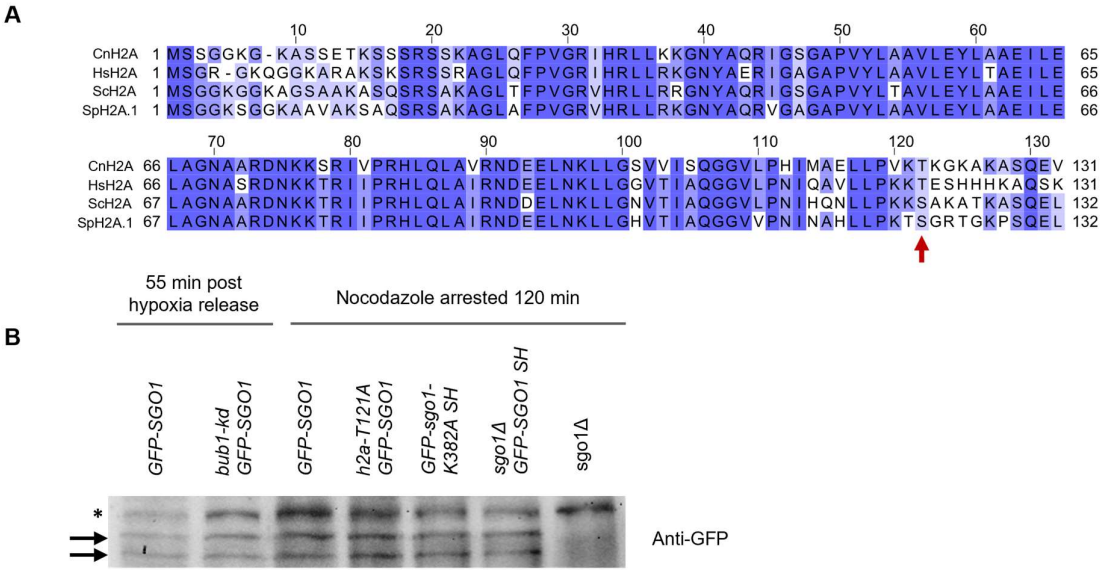

Supplementary Figure 10. Conservation of histone H2A sequence in *C. neoformans* and expression levels of GFP-Sgo1 in various mutant strains. (A) Multiple sequence alignment of H2A homologs obtained from *C. neoformans* (Cn), *S. cerevisiae* (Sc), *S. pombe* (Sp) and *H. sapiens* (Hs). The alignment was performed using Clustal Omega (Sievers et al., 2011) and formatted using Jalview 2 (Waterhouse et al., 2009). The dark blue shaded regions represent highly conserved amino acid residues. Arrow indicates the conserved T121/S120 residue phosphorylated by Bub1. **(B)** Western blot showing the expression levels of GFP-Sgo1 at metaphase in the indicated strains. * Indicates non-specific band used as a loading control. Arrows indicate two bands of GFP-Sgo1. *sgo1Δ* lane represents no tag control.

Supplementary Figure 11. *Polisetty et. al*

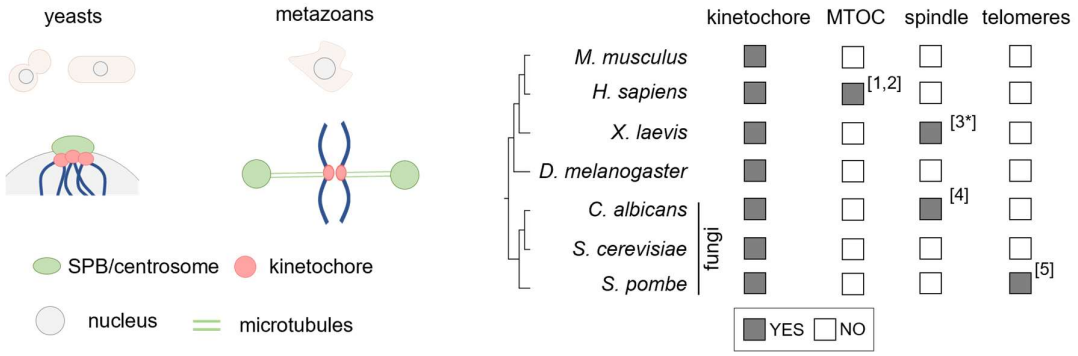

Supplementary Figure 11. Schematic highlighting the sub-cellular localization of shugoshin reported in various species. *Left*, schematic highlighting the spatial positioning of SPB/centrosome and centromeres in yeasts and metazoans. *Right*, localization of shugoshin with respect to the kinetochore, MTOCs (centrosomes or SPBs), spindle MTs, and telomeres. Filled and open squares represent the presence or absence of shugoshin at the indicated sub-cellular locations. The data was compiled from reviews (Marston, 2015, Gutierrez-Caballero et al., 2012). [1,2] (Mohr et al., 2015, Wang et al., 2008), [3*] (Salic et al., 2004), this study has shown that the purified N-terminal region of shugoshin is capable of binding to MTs *in* vitro. [4] (Sane et al., 2021) and [5] (Tashiro et al., 2016).